

1 **Mycobacterium tuberculosis reactivates HIV via exosomes mediated**
2 **resetting of cellular redox potential and bioenergetics**

3

4 Priyanka Tyagi^{1,2}, Virender Kumar Pal¹, Sandhya Srinivasan³, and Amit
5 Singh^{1*}

6 ¹Department of Microbiology and Cell Biology, Centre for Infectious Disease
7 Research, Indian Institute of Science (IISc), Bangalore-12

8 ²International Centre for Genetic Engineering and Biotechnology (ICGEB),
9 New Delhi-67

10 ³Vproteomics, New Delhi-16

11

12 Keywords: Exosomes, glutathione, redox potential, extracellular acidification
13 rate, oxidative phosphorylation, roGFP

14

15

16 * Correspondence:

17 Amit Singh, Ph.D

18 Associate Professor

19 Wellcome Trust-India Alliance Senior Fellow

20 Department of Microbiology and Cell Biology (MCBL)

21 Centre for Infectious Disease and Research (CIDR)

22 Indian Institute of Science (IISc)

23 Bangalore-12

24 asingh@iisc.ac.in

25 Ph: +918022932604

26 **Abstract**

27 The synergy between *Mycobacterium tuberculosis* (*Mtb*) and HIV-1 interferes
28 with therapy and facilitates pathogenesis of both human pathogens.
29 Fundamental mechanisms by which *Mtb* exacerbates HIV-1 are not clear.
30 Here, we show that exosomes secreted by macrophages infected with *Mtb*,
31 including drug-resistant clinical strains, reactivate HIV-1 by inducing oxidative
32 stress. Mechanistically, *Mtb*-specific exosomes realign mitochondrial and non-
33 mitochondrial oxygen consumption rate (OCR) and modulates the expression
34 of genes mediating oxidative stress response, inflammation, and HIV-1
35 transactivation. Proteomics revealed the enrichment of several host factors
36 (e.g., HIF-1 α , galectins, Hsp90) known to promote HIV-1 reactivation in the
37 *Mtb*-specific exosomes. Treatment with a known antioxidant, N-acetyl
38 cysteine, or with the inhibitors of host factors galectins and Hsp90 attenuated
39 HIV-1 reactivation by *Mtb*-specific exosomes. Our findings uncovered new
40 paradigms for understanding the redox and bioenergetics basis of HIV-TB co-
41 infection, which will enable the design of effective therapeutic strategies.

42

43

44

45

46

47

48

49

50

51 **Introduction**

52 Tuberculosis (TB) and Human Immunodeficiency Virus/Acquired
53 Immunodeficiency Syndrome (HIV/AIDS) jointly represent the major burden of
54 infectious diseases in humans worldwide. HIV-1/*Mtb* co-infected patients
55 exhibit rapid progression to AIDS and shorter survival kinetics [1]. Moreover,
56 the risk of acquiring active TB infection increases from 10% in a lifetime to
57 10% per year in the case of HIV-1 infected patients [2]. In 2015 alone, WHO
58 estimated that almost 11% of 10.4 million TB patients are also infected with
59 HIV-1, and one in every three deaths between HIV-1 infected individuals was
60 due to TB (http://www.who.int/hiv/topics/tb/about_tb/en/). Epidemiological
61 studies clearly indicate that both these human pathogens interact to
62 accelerate disease severity and deaths [2].

63

64 Since infection with HIV-1 significantly increases the risk of TB
65 reactivation in individuals latently infected with *Mtb* [3], a great majority of
66 studies were focused on revealing how virus disorganizes TB granuloma [4],
67 impaired phagosomal killing [5], and alters T-cell based immunity to
68 exacerbates *Mtb* pathogenesis [6]. In contrast, whether *Mtb* influences exit of
69 HIV-1 from latency and its reentry into a productive life cycle remain poorly
70 studied. Because HIV-1 can persist in a latent state for decades and then
71 reactivates to cause immunodeficiency, our particular interest is to understand
72 the mechanism, if any, underlying *Mtb* induced reactivation of HIV-1 from
73 latency. Growing body of evidences suggest that infection with *Mtb* or its
74 component(s) (lipids and secretory proteins) promotes HIV-1 replication by
75 regulating processes such as inflammation, MHCII processing, Toll-Like

76 Receptors (TLRs) signaling, CXCR4/CCR5 expression, proinflammatory
77 cytokines/chemokines production, and activating transcriptional regulators
78 (NF- κ B, NFAT) of the long-terminal repeats (LTRs) of HIV [7-13].
79 Contradictory evidences showing inhibition of HIV-1 replication by *Mtb*
80 complicates our understanding of how two human pathogens interact at the
81 molecular level [14, 15]. Despite this, research specifically addressing how
82 *Mtb* modulates HIV latency and reactivation is, however, quite scarce. In this
83 context, reactive oxygen species (ROS) and modulation of central metabolism
84 are considered to be one of the main mechanisms regulating HIV-1
85 replication, immune dysfunction, and accelerated progression to AIDS [16].
86 Deeper studies in this direction revealed an important role for a major cellular
87 antioxidant, glutathione (GSH) [17]. Low GSH levels in HIV patients have
88 been shown to induce provirus transcription by activation of NF κ B, apoptosis
89 of CD4 T cells, and depletion of CD4 T cells [18]. Consequently,
90 replenishment of GSH is considered as a potential supplement to highly active
91 antiretroviral therapy (HAART) [19]. Recently, we have reported subtle
92 changes in the intracellular and subcellular redox potential of GSH (E_{GSH})
93 modulates HIV-1 replication cycle [20]. We discovered that oxidative stress
94 caused by a marginal increase in intracellular E_{GSH} (25 millivolts [mV]) is
95 sufficient to trigger HIV-1 reactivation from latently infected cells, raising the
96 potential of targeting HIV-1 latency by the modulators of cellular GSH
97 homeostasis [20]. Interestingly, markers of oxidative stress such as ROS/RNS
98 and lipid peroxidation have been shown to be elevated in active TB patients
99 [21]. Specifically, serum/cellular GSH was either depleted or oxidized in
100 human TB patients and in the lungs of guinea pigs infected with *Mtb* [21, 22].

101 Treatment with GSH precursor, N-acetyl cysteine (NAC), reversed oxidative
102 stress to reduce bacterial survival and tissue damage in guinea pigs [22].
103 Additionally, *Mtb* infection has recently been shown to influence carbon flux
104 through glycolysis and TCA cycle in infected macrophages [23]. This, along
105 with the recognized role of GSH homeostasis and glycolysis in HIV infection,
106 indicates that the two pathogens might synergies via affecting redox signaling
107 and metabolic phenotypes of the host. We explored this connection and
108 investigated if *Mtb* induces variation in the intracellular E_{GSH} and bioenergetics
109 to induce HIV-1 reactivation program. We anticipate that such a study has the
110 potential to overcome many of the deficiencies in our understanding of the
111 metabolic basis of HIV-TB co-infection and may enable high throughput
112 screen to identify small molecule modulators of redox/central metabolism to
113 potentiate the intervention strategies against HIV-TB co-infection.

114

115 In this study, we showed that macrophages infected with virulent *Mtb*,
116 including multi-drug resistant (MDR) and extensively drug-resistant (XDR)
117 clinical strains, release exosomes to induce substantial oxidative stress in
118 neighboring non-infected macrophages (bystander). Taking cues from these
119 findings, we showed that *Mtb* exploits the exosome-based mechanism to
120 communicate and reactivate latent HIV-1 from monocytic (U1) and
121 lymphocytic (J-Lat) cells. Mechanistically, *Mtb* specific exosomes alter gene
122 expression, redox metabolism, and bioenergetics of latent cells to promote
123 HIV-1 reactivation. Proteomic analysis of exosomes indicates that *Mtb*
124 infection transports several proteins associated with host cellular pathways

125 known to reactivate HIV-1 by perturbing redox metabolism, inflammation, and
126 immune response.

127

128 **Results**

129 ***Mtb* infection induces oxidative stress in bystander macrophages**

130 We exploited a non-invasive biosensor (Grx1-roGFP2) of GSH redox
131 potential (E_{GSH}) [24] to measure dynamic changes in the redox physiology of
132 human macrophages (U937) upon infection with a virulent strain of *Mtb*
133 (H37Rv). GSH is the most abundant low molecular weight thiol produced by
134 mammalian cells, therefore, E_{GSH} measurement provides a reliable and
135 sensitive indicator of the cytoplasmic redox state of macrophages [20, 24].
136 The biosensor shows an increase in the fluorescence excitation ratio at
137 405/488 nm upon oxidative stress, whereas a ratiometric decrease is
138 associated with reductive stress (Fig. 1A). The ratiometric changes can be
139 easily fitted into the modified Nernst equation to precisely calculate E_{GSH} [24].

140

141

142 U937 monocytes expressing cytosolic Grx1-roGFP2 (U937/Grx1-
143 roGFP2) were differentiated to macrophages using PMA and infected with
144 *Mtb* H37Rv (Fig. 1B). At various time-points post-infection, 405/488 ratios
145 were measured by flow cytometry to calculate intracellular E_{GSH} as described
146 [20]. We first confirmed the response of biosensor to a well-known oxidant
147 cumene hydroperoxide (CHP) and a cell-permeable thiol-reductant
148 dithiothreitol (DTT). As expected, the treatment of U937/Grx1-roGFP2 with
149 CHP increases 405/488 ratio, which corresponds to E_{GSH} of -240 mV and
150 treatment with a cell-permeable thiol-reductant dithiothreitol (DTT) decreases

151 405/488 ratio, which corresponds to E_{GSH} of -320 mV. (Fig. 1C-F). Next, we
152 examined the biosensor response upon infection with *Mtb* H37Rv. Uninfected
153 U937/Grx1-roGFP2 cells exhibit highly reduced cytoplasm (405/488 ratio ~
154 0.1-0.15 over-time; $E_{GSH} = -301 \pm 2$ mV) (Fig. 1G). In contrast, *Mtb* infection
155 gradually increases the biosensor oxidation ratio over time, which results in an
156 ~ +20 mV shift in E_{GSH} (-282 ± 2 mV) at 24 h p.i. (Fig. 1G).

157

158 In order to investigate the relative contribution of infected versus
159 uninfected cells on E_{GSH} of macrophage population, we assessed the
160 biosensor response of bystander and *Mtb* infected U937 macrophages. *Mtb*
161 cells stained with a lipophilic dye PKH26 were used to infect U937/Grx1-
162 roGFP2 at moi 10. About $42.75\% \pm 4.05$ of U937/Grx1-roGFP2 cells were
163 infected with PKH26-labeled *Mtb* (PKH⁺/GFP⁺) (Fig. 2A). Interestingly,
164 bystander U937 (PKH⁻/GFP⁺) showed a greater 405/488 ratio as compared
165 to infected cells (PKH⁺/GFP⁺) at each time point tested (Fig. 2B). At 24 h
166 p.i., E_{GSH} of bystander cells was -276 ± 2 mV as compared to E_{GSH} of -286 ± 2
167 mV in the case of *Mtb* infected cells (Fig. 2B). This suggests that the redox
168 physiology of infected and bystander macrophages are distinctly affected
169 during *Mtb* infection. Additionally, U937/Grx1-roGFP2 cells infected with *Mtb*
170 genetically expressing red-fluorescent protein (RFP:tdTomato) confirmed a
171 higher 405/488 ratio of bystander cells (RFP⁻/GFP⁺) as compared to
172 infected cells (RFP⁺/GFP⁺) (Fig. 2C). Infection of U937/Grx1-roGFP2 with
173 PKH labeled heat-killed *Mtb* (*Hk-Mtb*) did not increase oxidative stress in the
174 infected or bystander cells (Fig. 2D), indicating that processes such as
175 secretion of bioactive lipids or proteins are the likely modulators of

176 intramacrophage E_{GSH} . The secretory proteins of Esx-1 family of *Mtb* are
177 known to induce oxidative stress in the infected macrophages [25]. Agreeing
178 to this, the *Mycobacterium bovis* (BCG) strain, defective in secreting Esx-1
179 proteins, elicits marginal degree of biosensor oxidation in both infected or
180 bystander U937/Grx1-roGFP2 (Fig. 2E). Viable *Mtb*, *Hk-Mtb*, and BCG strains
181 were internalized to a comparable degree by U937 (Fig. S1), precluding the
182 influence of variations in the initial uptake rates on the E_{GSH} of macrophages.

183

184 Since HIV-1 infected individuals are frequently co-infected with the drug-
185 resistant strains of *Mtb* [26, 27], we assessed the impact of single drug-
186 resistant (SDR; BND320), multi-drug resistant (MDR; Jal2261 and Jal 1934)
187 and extensively drug-resistant (XDR; Myc 431) strains of *Mtb* isolated from
188 patients [28] on E_{GSH} of U937. Infection with BND320 induces an increase in
189 405/488 ratio of infected and bystander macrophages to a degree comparable
190 to *Mtb* H37Rv (Fig. 2F). However, infection with MDR and XDR strains
191 stimulated a significantly higher oxidative shift in E_{GSH} of bystander cells as
192 compared to infected U937 (Fig. 2G, 2H, and 2I), and also as compared to
193 bystander cells in case of infection with *Mtb* H37Rv (compare Fig 2B with Fig
194 2G, 2H, and 2I). Altogether, these results confirm that infection with *Mtb*
195 drives changes in E_{GSH} of infected and bystander U937 cells and that clinical
196 drug-resistant isolates are potent inducers of oxidative stress in macrophages.

197

198 **Reactivation of HIV-1 upon co-culturing with *Mtb* Infected macrophages**

199 HIV-1 infects multiple immune cells including macrophages,
200 lymphocytes, and dendritic cells, whereas macrophages are the major host

201 cells for *Mtb*. Therefore, how *Mtb* infected macrophages communicates with
202 HIV-1 infected cells of different origin remain unknown. The induction of
203 oxidative stress in bystander cells raised a possibility that *Mtb* infected
204 macrophages could reactivate virus by modulating redox physiology of
205 neighboring cells chronically infected with HIV-1. This communication can be
206 mediated either by direct cell-cell contact or often by bioactive soluble factors
207 (e.g., cytokines). To assess these possibilities, we set up a co-culturing
208 experiment wherein *Mtb* infected U937 macrophages were cultured with J-Lat
209 10.6 lymphocytes latently infected with HIV-1. The latent HIV-1 can be
210 reactivated by various stimuli such as phorbol esters [12-
211 Otetradecanoylphorbol-13-acetate (TPA)], prostratin, and TNF α [29]. The
212 integrated HIV-1 genome encodes GFP, which allows precise quantification of
213 HIV-1 reactivation using flow cytometry. As expected, pretreatment of J-Lat
214 with TNF α (10 ng/ ml) induced significant HIV-1 reactivation, which translated
215 into a greater percentage of GFP+ cells over time (Fig. S2A). Co-culturing of
216 *Mtb* infected U937 with J-Lat also showed a time-dependent increase in GFP+
217 cells, indicating HIV-1 reactivation (Fig. S2A). However, co-culturing with
218 either uninfected or *Hk-Mtb* infected U937 significantly attenuated the
219 induction of GFP from J-Lat cells (Fig. S3A). As an additional verification, we
220 examined the effect of co-culturing on a monocytic cell line (U1) of HIV-1
221 latency [30]. The U1 shows basal expression of two integrated copies of HIV-
222 1 genome, but gene expression and viral replication can be reactivated by
223 various stimuli such as PMA, TNF α , IFN- γ , GM-CSF [31]. We tracked HIV-1
224 reactivation by immuno-staining for HIV-1 core protein, p24 and quantified
225 using flow cytometer. First, we confirmed that PMA treatment reactivated HIV-

226 1 from U1 in a time-dependent manner (Fig. S3B). Second, similar to J-Lat
227 findings, HIV-1 reactivation was readily observed upon co-culturing of U1 cells
228 with U937 infected with *Mtb*, whereas co-culturing with uninfected U937
229 macrophages or *Hk-Mtb* infected U937 macrophages partially reactivated
230 HIV-1 (Fig. S2B).

231

232 To examine if this may be related to the release of soluble factors from
233 *Mtb* infected macrophages, we treated J-LAT cells with culture supernatants
234 derived from *Mtb* infected U937 macrophages at 24 h p.i. A time-dependent
235 increase in GFP expression was induced by the addition of supernatant (50%,
236 v/v) from *Mtb* infected U937 on to J-Lat cultures (Fig. 3A). Culture supernatant
237 (50%, v/v) from uninfected U937 or *Hk-Mtb* infected macrophages showed
238 diminished expression of GFP from J-Lat (Fig. 3A). Similar to J-Lat, treatment
239 of U1 cells with the supernatant derived from *Mtb* infected U937 macrophages
240 reactivated HIV-1 to the highest level as compared to supernatant from *Hk-*
241 *Mtb* infected or uninfected U937 (Fig. 3B). Marginal reactivation of HIV-1 by
242 the supernatant of uninfected U937 macrophage is perhaps due to the known
243 effect of PMA (used as a differentiating agent) on proinflammatory cytokines
244 secretion in the extracellular milieu [32]. Agreeing to this, supernatant from
245 undifferentiated U937 monocytes completely failed to resuscitate HIV-1 from
246 U1 and J-LAT (Fig. 3A and 3B). To decisively rule out the influence of PMA on
247 HIV-1 reactivation in our assays, we infected RAW264.7 murine macrophages
248 with *Mtb* and collected supernatant at 24 h p.i. As a control, the supernatant
249 was also collected from the uninfected RAW264.7 macrophages. Addition of
250 the supernatant from uninfected RAW264.7 was completely ineffective in HIV-

251 1 reactivation from U1 cells, whereas supernatant derived from *Mtb* infected
252 RAW264.7 was fully potent in reactivating HIV-1 (Fig. 3C).

253

254 **Exosomes derived from *Mtb* infected macrophages and mice reactivate**
255 **HIV-1**

256 Exosomes released from *Mtb* infected macrophages have been shown
257 to direct NFκB-mediated production of proinflammatory cytokines and
258 chemokines from bystander cells [33]. Since HIV-1 reactivation is
259 fundamentally dependent on NFκB and proinflammatory
260 cytokines/chemokines [34], we tested the role of exosomes in HIV-1
261 reactivation. To begin understanding this, we infected U937 and RAW264.7
262 macrophages with *Mtb* and treated infected macrophages with a well-known
263 inhibitor of exosome secretion, GW4869 [35]. At 24 h post-treatment with
264 GW4869, we collected supernatant and performed HIV-1 reactivation in J-Lat
265 and U1 as described earlier. As shown in figure 3D and 3E, HIV-1 reactivation
266 in J-Lat and U1 was observed in case of supernatant derived from *Mtb*
267 infected macrophages, whereas a significant reduction in HIV-1 reactivation
268 was detected in case of supernatant derived from GW4869 treated *Mtb*
269 infected macrophages (Fig. 3D and 3E). Furthermore, we have taken a third
270 cell line (J1.1 lymphocyte) latently infected with HIV-1 [36] and confirmed that
271 only the supernatant derived from *Mtb* infected macrophages reactivated HIV-
272 1 (as shown by *gag* qRT-PCR) as compared to supernatant from uninfected,
273 *Hk-Mtb*, and GW4869 treated macrophages (Fig. 3F). These results suggest
274 a role for exosomes secreted by *Mtb* infected macrophages in reactivating
275 HIV-1. Since supernatant-derived from *Mtb* infected U937 and RAW264.7

276 macrophages resulted in an identical degree of HIV-1 reactivation, further
277 experiments are conducted using RAW264.7 cells only. This was necessary
278 to rule out any artifactual influence of PMA used to differentiate U937
279 monocytes prior to infection with *Mtb*. Furthermore, exosomes derived from
280 *Mtb* infected RAW264.7 have been shown to possess immune-modulatory
281 properties comparable to exosomes isolated from the serum of *Mtb* infected
282 mice or humans [37].

283

284 We infected RAW264.7 with *Mtb* H37Rv, and at 24 h p.i., exosomes
285 were isolated. Transmission electron microscopy (TEM) confirmed the size of
286 exosomes to be 80-150 nm [n= 100] (Fig. 4A), which is consistent with the
287 previous studies [38]. Immuno-gold labeling with CD63 primary antibody
288 followed by TEM confirmed the presence of this classical exosomal marker on
289 the surface (Fig. 4B) [39]. Immuno-blot analysis for exosome-specific markers
290 such as Rab5b, Alix, and CD63 established their enrichment on the exosomal
291 fraction relative to cell lysate (Fig. 4C). LAMP2 was present in both the
292 fractions as previously shown (Fig. 4C) [39]. Finally, we demonstrated that the
293 pretreatment of *Mtb* infected RAW264.7 macrophages with GW4869
294 significantly reduced the release of exosome as revealed by the loss of CD63
295 marker as compared to untreated or *Mtb* infected RAW264.7 macrophages
296 (Fig. 4D). Altogether, we confirmed the isolation of exosomes from *Mtb*
297 infected macrophages for investigating redox-dependent activation of HIV-1.

298

299 Various concentrations of exosomes isolated from *Mtb* infected
300 RAW264.7 macrophages were used to treat U1 and HIV-1 reactivation was

301 measured by p24 immuno-staining and qRT-PCR of *gag* transcript. As
302 compared to uninfected control, *Mtb* specific exosomes significantly induce
303 HIV-1 reactivation from U1. Both p24 staining and *gag* qRT-PCR displayed ~
304 4-fold increase as compared to uninfected control (Fig. 4E, 4F, and 4G).
305 Exosomes isolated from macrophages infected with *Hk-Mtb* were ineffective
306 in reactivating HIV-1 (Fig. 4E, 4F, and 4G). However, the exosomes derived
307 from RAW264.7 macrophages infected with MDR and XDR strains of *Mtb*
308 were equally potent in reactivating HIV-1 (Fig. 4H and 4I). Finally, to
309 conclusively show that exosomes derived from *Mtb* infection reactivate HIV-1,
310 we treated U1 with exosomes isolated from serum and lungs of mice
311 chronically infected with *Mtb* and stained for p24. In both cases, we observed
312 a significant reactivation (~ 5-fold) of HIV-1 as compared to exosomes
313 isolated from uninfected animals. (Fig. 4J and 4K) However, exosomes
314 isolated from *Mtb* infected lungs reactivated HIV-1 at a lower concentration
315 than serum (Fig. 4J and 4K). Taken together, our data suggest that exosomes
316 could be one of the important mediators of HIV-1 reactivation during *Mtb*
317 infection.

318

319 **Exosomes from *Mtb* infected macrophages modulate redox potential** 320 **and host gene expression of U1 cells**

321 Elevated ROS, RNI, and depletion/oxidation of intracellular thiols
322 (cysteine, thioredoxin, GSH) were shown to activate the HIV-1 long terminal
323 repeat (LTR) through the redox-responsive transcription factor NFκB [40, 41].
324 Therefore, we first tested if exosomes derived from RAW 264.7 infected with
325 various *Mtb* strains induce oxidative stress to reactivate HIV-1. Treatment of

326 U1/Grx1-roGFP2 with exosomes derived from RAW 264.7 infected with *Mtb*
327 H37Rv, MDR, and XDR strains uniformly increases biosensor ratio at 24 h
328 and 48 h post-treatment, indicating oxidative stress (Fig. 5A). As expected,
329 exosomes derived from uninfected or *Hk-Mtb* infected RAW 264.7 failed to
330 induce oxidative stress in U1 cells (Fig. 5A). To show that exosomes-triggered
331 oxidative shift in E_{GSH} precedes HIV-1 reactivation, we pretreated U1 cells
332 with the GSH-specific antioxidant, N-acetyl cysteine (NAC), followed by
333 exosomes addition. Treatment with NAC entirely abrogated the potential of
334 *Mtb* specific exosomes to reactivate HIV-1 in a concentration dependent
335 manner (Fig. 5B). This result reiterates that oxidative stress is likely to be an
336 important mechanism induced by *Mtb*-specific exosomes to reactivate HIV-1.

337

338 To further understand the mechanism of exosomes mediated HIV-1
339 reactivation, we examined the influence of *Mtb* specific exosomes on host
340 gene expression using NanoString nCounter gene expression analysis. This
341 technology permits for the absolute quantification of a large number of RNA
342 transcripts without any requirements for reverse transcription or DNA
343 amplification [42]. From the NanoString panel, we focused on host genes that
344 respond to HIV replication (e.g., HIV receptors-ligands, proteins involved in
345 HIV replication, inflammatory response, apoptosis, cell cycle, and transcription
346 activators of HIV LTR) as well as genes involved in oxidative stress response
347 (Table S1a-S1c). Exosomes derived from uninfected or *Mtb* (live or *Hk*)
348 infected RAW 264.7 macrophages were used to treat U1 and total RNA was
349 isolated at 12 h post-treatment. An early time point is taken to ensure that we
350 capture gene expression changes that precede HIV-1 reactivation upon

351 exosomes challenge. Also, at a later time point, the primary effect of
352 exosomes can be masked due to transcriptional changes in response to HIV
353 proliferation and associated cytopathic consequences. PMA treated U1 were
354 taken as a positive control. Consistent with our biosensor data, treatment with
355 viable *Mtb*-specific exosomes induces genes encoding components of
356 superoxide-producing enzyme- NADPH oxidase (e.g., cytochrome B-245 Beta
357 chain [CYBB], NCF1, and NCF2) (Fig. 5C). As a consequence, several genes
358 involved in mitigating ROS and maintaining redox balance such as PRDX2
359 (peroxiredoxin) [43], TXNRD1 (thioredoxin reductase 1) [44], sodium-
360 dependent cysteine-glutamate antiporter (SLC7A11) [45], and ferritin (FTH1)
361 [46] were highly induced in U1 treated with *Mtb*-exosomes than *Hk-Mtb* or
362 uninfected exosomes (Fig. 5C). Additionally, a gene encoding heme
363 oxygenase 1 (HMOX1) is highly induced in U1 treated with *Mtb*-exosomes
364 (Fig. 5C). HMOX1 is involved in heme catabolism and its dysregulation and
365 polymorphism in its promoter are linked with HIV- associated neurocognitive
366 disorder [47]. Gene encoding a member of the selenoprotein family (VCP-
367 interacting membrane protein [VIMP], also known as selenoprotein S was
368 induced by *Mtb*-exosomes (Fig. 5C). VIMP is a redox-sensing protein that
369 regulates inflammation by mediating cytokine production [48], suggesting that
370 VIMP can coordinate HIV-1 reactivation by triggering an inflammatory reaction
371 in response to oxidative stress induced by *Mtb*-exosomes.

372

373 In agreement with HIV-1 reactivating potential of *Mtb*-exosomes, genes
374 involved in ensuring HIV-1 LTR activation were induced. For example,
375 NFkBIA and SQSTM1/P62 involved in the activation of transcription factor

376 NF κ B were upregulated [49](Fig. 5C). Another transcription factor FOS, which
377 reactivates HIV-1 [50], was also upregulated by *Mtb*-exosomes. Several
378 genes encoding host inflammatory mediators were induced by *Mtb*-
379 exosomes. For examples, expression of CXC chemokine subfamily (CXCL8),
380 monocyte chemoattractant protein 1 (MCP1; CCL2) and macrophage-
381 inflammatory-protein-1 alpha (MIP-1a; CCL3) showed greater expression in
382 U1 treated with *Mtb* specific exosomes as compared to *Hk-Mtb* or uninfected
383 exosomes (Fig. 5C). All of these factors are well known to facilitate HIV-1
384 infection and promote replication in macrophages [51]. In facts, higher levels
385 of CCL2 were detected in the bronchoalveolar lavage (BAL) fluid of pulmonary
386 TB patients and pleural fluid of HIV-1 infected patients, indicating the
387 importance of this proinflammatory cytokine in HIV-TB co-infection [52].
388 Interestingly, apolipoprotein B mRNA-editing enzyme catalytic polypeptide-like
389 3G (APOBEC3G), a known HIV restriction factor [53], was also induced by *Mtb*-
390 exosomes. In addition to viral restriction, APOBEC3G activity also promotes
391 heterogeneity in HIV sequence resulting in HIV phenotypes with greater capacity
392 to escape immune pressures [54]. Therefore, it's likely that co-infection with *Mtb*
393 and subsequent exosomes release can accelerate APOBEC3G mediated
394 generation of more fit viral variants. Consistent with this, pleural fluid
395 mononuclear cells (PFMCs) from HIV/TB coinfecting patients show higher
396 expression of APOBEC3G [55]. Lastly, gene encoding serpin peptidase
397 inhibitor, clade C (SERPINC1; antithrombin) that induces at very early stages
398 of HIV-1 replication, and is a component of the viral core [56], was
399 upregulated by *Mtb* exosomes (Fig. 5C). We found a striking similarity
400 between the transcriptional signatures of host genes induced by *Mtb*-
401 exosomes to those induced by the PMA treatment (Fig. 5D), confirming that

402 *Mtb*-exosomes are eliciting host response associated with HIV-1 reactivation.

403 Taken together, exosomes released by *Mtb* infected macrophages modulate

404 host redox metabolism and inflammatory response to ensure HIV-1

405 reactivation.

406

407 **Influence of *Mtb*-specific exosomes on oxidative phosphorylation**

408 **(OXPHOS) of U1 cells**

409

410 We have previously shown that HIV-1 reactivation precedes an oxidative

411 shift in mitochondrial E_{GSH} and the mitochondrial redox physiology closely

412 coincides with the progression of HIV disease [20]. This indicates that *Mtb*-

413 exosomes might influence the mitochondrial physiology of HIV infected cells

414 to promote oxidative stress and viral replication. To examine this possibility,

415 we performed a real-time assessment of the mitochondrial function of U1 cells

416 in response to *Mtb*-specific exosomes. We quantified mitochondrial

417 physiology by measuring several key parameters associated with oxidative

418 phosphorylation (OXPHOS) using Seahorse XF Flux technology (Fig. 6A).

419

420 Several parameters of mitochondrial respiration, including basal

421 respiration (Basal-Resp), ATP-linked respiration, proton leak and spare

422 respiratory capacity (SRC), were derived by the successive addition of

423 pharmacological agents to the exosomes challenged U1 cells, as outlined in

424 Figure 6A. To determine each parameter, three reiterated rates of oxygen

425 consumption (OCR) are made over an 80-minute period. Firstly, baseline

426 cellular oxygen consumption (OCR) is measured, from which Basal-Resp is

427 derived by subtracting non-mitochondrial respiration. Secondly, an inhibitor of
428 complex V (oligomycin) is added, and the resulting OCR is used to calculate
429 ATP-linked OCR (by deducting the OCR after oligomycin addition from
430 baseline cellular OCR) and proton leak (by subtracting non-mitochondrial
431 respiration from the OCR upon oligomycin addition). Thirdly, maximal
432 respiration (Max Resp), which is the change in OCR after uncoupling ATP
433 synthesis from electron transport by adding carbonyl cyanide-4-
434 (trifluoromethoxy)phenylhydrazone (FCCP). Lastly, antimycin A, a complex III
435 inhibitor, and rotenone, a complex I inhibitor, are added together to inhibit
436 ETC function, revealing the non-mitochondrial respiration (Non-Mito Resp).
437 The spare respiratory capacity (SRC) is calculated by subtracting basal
438 respiration from maximal respiratory capacity.

439

440 U1 cells were treated with exosomes isolated from RAW264.7 infected
441 with viable or *Hk-Mtb* for 48 h. Following this, U1 cells were seeded on to the
442 XF cartridge plates and subjected to the mitochondrial stress test to measure
443 various OXPHOS parameters as described earlier. As compared to exosomes
444 from uninfected macrophages, treatment of U1 cells with *Mtb*-specific
445 exosomes significantly decreased various respiratory parameters including
446 basal respiration, ATP-linked OCR, and H⁺ leak (Fig. 6B and 6D). In contrast,
447 the non-Mitochondrial Resp was significantly increased, whereas SRC was
448 not significantly affected (Fig. 6B and 6D). Exosomes derived from
449 macrophages infected with *Hk-Mtb* modulate OXPHOS parameters
450 comparable to exosomes from uninfected macrophages (Fig. 6C and 6E). The
451 contrasting influence of viable and *Hk-Mtb* exosomes on Basal-Resp, ATP-

452 linked OCR and proton leak indicate a profound deceleration of respiration of
453 U1 upon reactivation of HIV-1 by *Mtb* exosomes. Generation of ROS (e.g.,
454 superoxide) is an inevitable consequence of normal mitochondrial respiration.
455 Since *Mtb* exosomes induce an oxidative shift in E_{GSH} of U1, a decrease in
456 Basal-Resp and ATP-linked OCR could be a cellular strategy to avoid
457 overwhelming oxidative stress. This would ensure successful HIV-1
458 reactivation without triggering the detrimental effects of ROS on U1. Agreeing
459 to our findings, active HIV-1 replication depends largely on increased
460 glycolytic flux rather than OXPHOS to meet the surge in biosynthetic and
461 bioenergetics demand [57].

462

463 Our OXPHOS results also provide clues about the mechanism of an
464 oxidative shift in E_{GSH} upon HIV reactivation by exosomes. We observed a
465 significant increase in non-mitochondrial O_2 consumption in the case of U1
466 treated with *Mtb* specific exosomes (Fig. 6D and 6E). Non-mitochondrial O_2
467 consumption is usually due to activities of enzymes associated with
468 inflammation such as lipoxygenase, cyclo-oxygenase, and NADPH oxidase
469 [58]. Consistent with this, our NanoString data showed an increased
470 expression of genes encoding various components of the NADPH oxidase
471 complex. Altogether, HIV-1 reactivation by *Mtb*-specific exosomes was
472 associated with a marked change in OXPHOS parameters including a
473 reduced basal OCR and ATP-linked OCR. An increased Non-Mito OCR is
474 likely responsible for the generation of oxidative stress during HIV-TB co-
475 infection.

476

477 **Proteomics of exosomes released upon *Mtb* infection**

478 Having established that *Mtb* specific exosomes reactivate HIV-1 by
479 modulating redox and bioenergetics, we sought to determine the content of
480 exosomes. Mycobacterial components (e.g., lipids, proteins, and RNA) that
481 exert pro-inflammatory responses are consistently enriched in the exosomes
482 of *Mtb* infected macrophages [59, 60]. However, the identity of host proteins
483 within exosomes isolated from *Mtb* infected macrophages remains
484 uncharacterized. This is important as immune-activated macrophages secrete
485 several redox-signaling proteins involved in eliciting proinflammatory response
486 and oxidative stress in the neighboring cells [43]. On this basis, we reasoned
487 that profiling of exosome-associated host-proteins likely shed new insight on
488 how *Mtb* induces HIV-reactivation.

489

490 We identified proteins associated with exosomes from uninfected, live
491 *Mtb*, and *Hk Mtb* infected RAW264.7 cells using LC-MS/MS (Fig. 7A). In total,
492 4953 proteins were identified in all three samples with two-biological
493 replicates (Sequest Program, Fig. 7A, Table S2). As expected, a high
494 correlation value (> 0.90 , Pearson correlation coefficient) was observed within
495 the two biological replicates from the same group than unrelated groups (0.6-
496 0.7) (Fig. S3C). About 80 of the 100 most identified exosomal proteins of the
497 ExoCarta database were identified in our dataset. While ~3250 proteins
498 overlapped among the three groups, we discovered that 86, 298, and 142
499 proteins were exclusively present in the uninfected, live *Mtb*, and *Hk Mtb*,
500 respectively (Fig. S3B). The highest numbers of proteins in case of live *Mtb*
501 exosomes clearly indicates that *Mtb* infection promotes secretion of proteins

502 in exosomes. Analysis of differentially expressed proteins (Table S3a-S3c)
503 (log 2 fold, $P \leq 0.01$) showed that in comparison to uninfected samples, 436
504 proteins were up-regulated and 290 were down-regulated in live *Mtb*-
505 exosomes (Fig. 7B). Similarly, 390 proteins were induced and 337 were
506 repressed in *Hk-Mtb* as compared to uninfected samples (Fig. 7B). Direct
507 comparison of live versus *Hk-Mtb* revealed that ~ 40 proteins were
508 differentially enriched in exosomes derived from live *Mtb* infected
509 macrophages (Fig. 7B). This suggests that live *Mtb*-derived exosomes contain
510 different proteins, which might mediate more specific function such as redox
511 imbalance and HIV reactivation upon secretion.

512

513 Biological process analysis of Gene ontology (GO) showed that the
514 differentially expressed proteins belong to diverse categories including
515 cellular/metabolic processes, biological regulation and response to stimulus
516 (Fig. S4). Molecular function analysis of GO revealed that most of the proteins
517 carry out binding and catalytic activity, indicating their roles in exosomes
518 cargo sorting, release, and uptake by the recipient cells (Fig. S5). This is
519 further confirmed by cell component analysis wherein exosomal proteins
520 mainly belonged to cell organelle, membrane, and macromolecular complexes
521 involved in exosome biogenesis (Fig. S5) (Table S4a-S4c, S5a-S5c, S6a-
522 S6c).

523

524 Next, we classified the differentially expressed proteins of each group by
525 KEGG signaling pathway (Table S7) of KEGG database (Fig. 7C). *Mtb*
526 exosomes were found to be enriched with proteins involved in glycolysis,

527 gluconeogenesis, fructose and mannose metabolism, galactose metabolism,
528 pentose phosphate pathway (PPP), cysteine and methionine metabolism.
529 Increased oxidative stress in HIV infected patients is associated with higher
530 glucose utilization and deficiency of cysteine and methionine [61-63].
531 Enrichment of sugar metabolic enzymes in *Mtb* exosomes possibly assists in
532 HIV-1 reactivation by fueling ATP generating processes for the energy
533 consuming functions such as virus transcription, translation, packaging, and
534 release. Similarly, cysteine metabolism serves as a source of GSH
535 biogenesis, while PPP enzymes provides NADPH for regenerating GSH from
536 GSSG. Both of these activities are essential for alleviating excessive oxidative
537 stress to avoid cell death during HIV-1 reactivation [16]. We observed
538 enrichment of proteins coordinating RNA transport/quality control, DNA
539 replication, and cell cycle, all of which are important for the reactivation of
540 HIV-1 [64, 65]. Importantly, estrogen signaling proteins involved in induction of
541 mitochondrial ROS and HIV-1 reactivation are enriched in *Mtb*-exosomes [66,
542 67]. HIF-1 signaling plays an important role in HIV-1 pathogenesis by
543 facilitating viral replication and promoting lymphocyte and macrophage
544 mediated inflammatory response [68]. HIF-1 pathway proteins are specifically
545 induced in *Mtb* exosomes (Fig. 7C).

546

547 We discovered that several members of heat shock protein family (HSP)
548 and galectins were exclusively enriched in *Mtb* exosomes. *Mtb* infected
549 macrophages are reported to secrete HSPs in exosomes to induce
550 proinflammatory response (NF κ B and TNF α) from the uninfected bystander
551 cells [69]. Furthermore, HSP such as Hsp90 potently reactivates HIV from

552 latently infected cell lines and CD4+ T cells [70]. Likewise, galectins are
553 consistently associated with oxidative stress, inflammation, and HIV-1
554 reactivation [71, 72]. Finally, STAT-1 of JAK-STAT signaling pathway, which
555 is well known to modulate HIV replication cycles, was enriched in *Mtb*-specific
556 exosomes [73, 74].

557

558 Altogether, infection with viable *Mtb* induces secretion of specific
559 proteins in exosomes to reactivate HIV-1 by affecting redox, central
560 metabolism, and inflammatory responses.

561

562 **HSPs and Galectins facilitate HIV-1 reactivation by *Mtb* exosomes.**

563 Since multiple pathways are likely to synergies during HIV-1
564 reactivation by *Mtb* specific exosomes, determination of the specific
565 proteins/pathways in this process is challenging. However, to begin
566 delineating the role of some of the components secreted in exosomes upon
567 *Mtb* infection in HIV-1 reactivation, we decided to examine the effect of HSPs
568 and galectins. We first examined the effect of Hsp90 pathway by using a
569 specific inhibitor of Hsp90- 17-(N-allylamino)-17-demethoxygeldanamycin (17-
570 AAG) [70]. The inhibitor 17-AAG binds to ATPase pocket of HSP90 and
571 compete with ATP, resulting in inactivation of chaperone function [70]. U1
572 cells were stimulated with PMA and HIV-1 reactivation was monitored in the
573 presence or absence of 17-AAG by scoring for p24 positive cells using flow
574 cytometry. The 17-AAG completely abolished PMA-mediated HIV-1
575 reactivation but showed no effect on the basal expression of p24 in the

576 unstimulated cells (Fig. 8A). Similarly, 17-AAG significantly decreased HIV-1
577 reactivation in U1 by *Mtb*-specific exosomes (Fig. 8B).

578

579 To understand how galectins modulate exosomes mediated reactivation
580 of HIV-1, we exploited the lactose binding property of galectins. Galectins
581 form a complex with lactose, via carbohydrate binding domain, which inhibits
582 galectins activities [75]. Galectins control numerous biological functions
583 mainly by binding to the cell surface associated glycoproteins or glycolipid
584 receptors. Therefore, we thought of inhibiting the activity of galectins before
585 it's transported in the *Mtb*-specific exosomes to preclude its interaction with
586 the U1 cell surface glycoproteins/receptors. To do this, we treated *Mtb*
587 infected RAW 264.7 macrophages with 50 and 100 mM of lactose for 24 h
588 and exosomes were isolated. These exosomes were then used to reactivate
589 HIV-1 in U1. As shown in figure 8C, exosomes isolated from the lactose
590 treated cells significantly reduced the ability of *Mtb*-specific exosomes to
591 reactivate HIV-1 from U1 monocytes. Altogether, *Mtb*-specific exosomes
592 harbor and convey cellular effectors responsible for reversing viral latency in
593 cell lines chronically infected with HIV-1.

594

595

596 **Discussion**

597 We have previously shown that a marginal oxidative shift in E_{GSH} is
598 sufficient to reactivate HIV-1 [20]. Others have shown that *Mtb* induces
599 oxidative stress and GSH imbalance in the infected macrophages, animals,
600 and humans [21, 22]. HIV-TB co-infected patients suffer from glutathione

601 stress, metabolic deficiencies, and immune-dysfunction [21]. Critically, we
602 now made an effort to unify in a coherent picture of these separate
603 observations, establishing a functional link between *Mtb* induced oxidative
604 stress and HIV-1 reactivation from latency, which may have therapeutic
605 implications. Furthermore, we provide evidence for oxidative stress-mediated
606 HIV-1 reactivation, which relies on the secretion of biological effectors present
607 in the exosomes released from *Mtb* infected macrophages. Although with
608 hindsight the connection between *Mtb*, oxidative stress and HIV-1 reactivation
609 might appear obvious, intracellular redox metabolism is dependent on many
610 pathways, and HIV-1 reactivation is a multifactorial process, hence we expect
611 multiple mechanisms where redox might be interlinked. In fact, our
612 NanoString data suggest that the effect of *Mtb*-specific exosomes on HIV
613 reactivation is likely mediated by diverse genetic factors. For example, gene
614 expression data indicate that superoxide generation by NADPH oxidase could
615 be one of the factors contributing to an oxidative shift in E_{GSH} and HIV-1
616 reactivation upon treatment with exosomes. However, the induction of several
617 genes encoding antioxidant enzymes contradicts the requirement of ROS for
618 viral reactivation. It appears that cells attempt to mitigate excess ROS to
619 ensure exosome-mediated HIV-1 reactivation without triggering global ROS-
620 mediated cytotoxicity. Consistent with this, treatment with *Mtb*-specific
621 exosomes induces only a modest oxidative shift in E_{GSH} (-276 mV) of U1.
622 Similar oxidative changes in E_{GSH} were earlier found to uniformly reactivate
623 HIV-1 from latency without affecting viability [20]. Low levels of ROS are
624 known to activate HIV LTR via activation of NFκB. Agreeing to this,
625 expression data confirm the induction of NFκBIA and SQSTM1/P62 involved

626 in NFKB activation upon exosome treatment. The induction of AP-1 (FOS),
627 which is activated by ROS and reactivates HIV-1 [50], also indicate that
628 exosomes-promoted oxidative stress acts as a critical cue to reactivate HIV-1
629 via redox-sensitive transcription factors. This explanation aligns well with the
630 ability of the antioxidant, NAC, in subverting HIV-1 reactivation by exosomes.

631

632 Recently, several studies have examined the contribution of metabolic
633 indicators (OXPHOS and glycolysis) in determining susceptibility to HIV-1
634 infection and replication [57, 62]. Overall, these studies revealed the
635 requirements of high OXPHOS and glycolysis rates for HIV-1 infection and
636 continued replication [57]. In contrast, quantification of respiratory and redox
637 parameters during HIV-1 reactivation is lacking. In this context, our data
638 indicate a critical role of oxidative stress in reactivating HIV-1 by *Mtb*
639 exosomes. Consistent with this, a recent study demonstrated that exosomes
640 from *Mtb* infected neutrophils trigger superoxide production in macrophages
641 [76]. However, the mechanism of superoxide generation remains
642 uncharacterized. Since the respiratory chain is the major site for generation of
643 ROS such as superoxide, cell flux assays showing *Mtb* exosome-mediated
644 deceleration of mitochondrial OCR provide new mechanistic insight. It is well
645 known that reduced mitochondrial OCR leads to build up of NADH, which
646 results in trapping of flavin mononucleotide (FMN) in the reduced state on
647 complex I of the electron transport chain [77]. Reduced FMN has been
648 consistently shown to donate one electron to O₂ resulting in the generation of
649 superoxide by complex I [77]. Other sites in mitochondria, which communicate
650 with NADH and coenzyme Q (COQ) pools such as complex III and α-

651 ketoglutarate dehydrogenase, also produce superoxide and H₂O₂ during slow-
652 down of OCR [77].

653

654 We discovered that contrary to mitochondrial OCR, non-mitochondrial
655 OCR is significantly induced by *Mtb*-specific exosomes, which links oxidative
656 stress with the enzymatic activities unrelated to mitochondria (e.g., NADPH
657 oxidase, lipoxygenase, and cyclo-oxygenase) as ROS sources [58]. All of
658 these enzymes are influenced by HIV infection and are well known to
659 generate ROS and influence GSH homeostasis [78-80]. Importantly, a recent
660 study showed that the treatment of bone marrow-derived macrophages
661 (BMDM) with exosomes derived from *Mtb* infected macrophages increases
662 recruitment of NADH oxidase on the phagosomes [60]. Taken together, data
663 suggest that both mitochondrial and non-mitochondrial mechanisms
664 associated with oxygen consumption likely mediate ROS generation and HIV-
665 1 reactivation by *Mtb* exosomes.

666

667 Exosomes isolated from *Mtb* infected macrophages contain bacterial
668 lipids, proteins, and RNA, which stimulate a pro-inflammatory response in
669 bystander macrophages. Our study updated this knowledge by including the
670 potential of *Mtb* exosomes in modulating redox and bioenergetics of
671 uninfected bystander cells, which affects HIV-1 latency and reactivation
672 program. Rather than mycobacterial components, which are well
673 characterized, we focused on identifying the macrophage proteins enriched in
674 *Mtb* exosomes to understand the contribution of the host on virus reactivation.
675 Various proteins associated with host pathways mediating HIV-1 reactivation

676 were enriched in *Mtb* exosomes. Secretion of HSP90 along with its co-
677 chaperone Cdc37 and galectins were found to be important for *Mtb* exosomes
678 mediated virus reactivation. HSP90 is abundantly present in the serum of HIV-
679 TB co-infected patients [81]. Galectins such as Gal3 secretes in exosomes
680 [82] and promotes redox imbalance [83], whereas Gal9 is frequently found in
681 the plasma of TB patients [84] and reactivates HIV-1 [71]. While we have
682 characterized the proteome of *Mtb*-exosomes derived from macrophages, it is
683 certain that the presence of immuno-modulatory proteins, lipids, and RNA of
684 *Mtb* will also influence HIV-1 reactivation.

685

686 Our findings have therapeutic implications. For example, HSP90
687 inhibitor, SNX-5422, shows a good safety profile in patients with solid tumors
688 [85]. One can envisage using these inhibitors along with HAART to repress
689 HIV-1 reactivation and replication in HIV-TB co-infected patients, at least in
690 early stages of post-infection, when the viral reservoir is small. Furthermore,
691 reactivation of latent virus coupled with HAART has been put forward as a
692 possible “Kick-and-Kill” approach to eliminate latent reservoir. However, most
693 of the screening efforts identified latency-reversing agents that are cytotoxic.
694 Since the *Mtb*-specific exosomes mediate HIV-1 reactivation without causing
695 overwhelming oxidative stress, we anticipate that co-treatment of *Mtb*
696 exosomes with HAART can target HIV-1 reservoir without triggering global
697 cytotoxicity. Exosomes derived from *Mtb* infected macrophages were already
698 reported to potentiate the antimycobacterial activity of anti-TB drugs *in vivo*
699 [60], suggesting that a combination of *Mtb* exosomes with HAART and/or anti-
700 TB drugs can be exploited to reduce the burden of HIV-TB co-infection.

701

702 In conclusion, we identified new paradigms in HIV-TB co-infection,
703 including the role of *Mtb* exosomes in inducing oxidative stress and
704 decelerating OXHPOS in the cells latently infected with HIV-1. These events
705 act as a signal to trigger a transcriptional response that promotes HIV-1
706 reactivation and inflammation. Identification of host factors enriched in *Mtb*
707 exosomes to mediate virus reactivation has direct implications on the
708 mechanism of HIV-1 reactivation and multiplication in HIV-TB co-infected
709 individuals. Thus, the quantifiable redox and respiratory parameters along
710 with the transcript and protein signatures established in this study would
711 enable direct assessment of future antimicrobials against HIV and TB
712 coinfection.

713

714

715 **Materials and methods**

716 **Cell lines, Bacterial cultures**

717 The human monocytic cell line U937, murine macrophage cell line
718 RAW264.7, chronically HIV-1 infected U1 (monocytic cell line) and J1.1 (T-
719 lymphocytic cell line) were cultured as described earlier [20, 86]. J-Lat 10.6
720 cells (Jurkat T-lymphocytic cell line, is a reporter cell line, containing a full-
721 length integrated HIV-1 genome with a non-functional *env* due to frame shift
722 and *gfp* in place of *nef* gene) were maintained in RPMI-1640 (Cell Clone)
723 supplemented with 10% heat inactivated Fetal Bovine Serum (Sigma Aldrich),
724 2 mM L-glutamine, 100 U/ml penicillin and 100 mg/ml streptomycin (Sigma
725 Aldrich) at 37°C and 5% CO₂. Bacterial strains used in this study are wild
726 type *Mycobacterium tuberculosis* H37Rv (*Mtb*), *Mycobacterium bovis* Bacillus

727 Calmette Guerin (BCG), single drug resistant (SDR) clinical isolate BND 320,
728 multiple drug resistant (MDR) clinical isolates Jal 1934, Jal 2261, and
729 extensively drug resistant (XDR) clinical isolate MYC 431 (kind gift from Dr.
730 Kanury V.S. Rao, ICGEB, New Delhi), were grown till mid log phase (OD_{600} of
731 0.8) as described previously [86]. For tdTomato expressing *Mtb* strains,
732 competent cells were prepared as described in [86] and were electroporated
733 using 1 μ g of the pTEC27 plasmid (pMSP12::tdTomato, kind gift from Prof.
734 Deepak Saini, IISc, Bangalore) with settings of 2.5 kV voltage, 25 μ F
735 capacitance and 1000 Ω resistance in Bio Rad Gene Pulser. Electroporated
736 bacilli were kept for overnight recovery in 7H9 followed by selection on 7H11
737 agar plates containing hygromycin (50 μ g/ml). After 21 days of selection,
738 bacteria were grown in 7H9 broth till mid-log phase and used for further
739 studies. For generating heat killed *Mtb* (*Hk-Mtb*), bacilli were killed by
740 resuspending the pellet in 2 ml of RPMI and heating it to 80 °C for 30 minutes
741 (min) using established protocol [87].

742

743 ***Mtb* labelling with PKH-26 GL, complement opsonization and infection**

744 Freshly grown *Mtb* bacilli were labelled with fluorescent lipophilic dye
745 PKH-26 GL (Sigma-Aldrich) as per the manufacturer's instructions to prepare
746 red labelled bacteria to distinguish between *Mtb* infected and bystander cells.
747 Briefly, pelleted *Mtb* bacilli were resuspended in 300 μ l of diluent C.
748 Fluorescent staining was performed at a final concentration of 10 μ M for 15
749 min at room temperature and fetal bovine serum (FBS) was added to
750 terminate the labelling process. Bacilli were then washed thoroughly three
751 times with 1X phosphate buffer saline (PBS) and resuspended in RPMI-1640

752 (Cell Clone). For complement opsonization *Mtb* bacilli were opsonized in 50%
753 human serum for 30 min at 37 °C as described [88] and then washed three
754 times in 1X PBS. For infection, U937 cells stably expressing Grx1-roGFP2 in
755 the cytosol were seeded at a density of 0.2 million per well in 24-well plates
756 and were differentiated into macrophages by a 24 h treatment with 5 ng/ml of
757 phorbol 12-myristate 13-acetate (PMA; Sigma-Aldrich Co. Saint Louis, MO,
758 USA). Cells were rested overnight following chemical differentiation to ensure
759 that they reverted to a resting phenotype before infection. Differentiated U937
760 cells were then infected with *Mtb* at multiplicity of infection (moi) 10 and
761 incubated for 4 h at 37 °C in 5% CO₂. Cells were then treated with amikacin at
762 200 µg/ml for 2 h to kill extracellular bacteria. After infection cells were
763 washed thoroughly with 1X PBS and resuspended in complete media (RPMI
764 supplemented with 10% FCS).

765

766 **Redox potential measurements**

767 The intracellular redox potential measurements were performed as
768 described previously [20]. Briefly, U937 cells stably expressing Grx1-roGFP2
769 in the cytosol were infected with PKH-26 labelled *Mtb*. At the indicated time
770 points, cells were treated with 10mM N-ethylmaleimide (NEM) for 5 min and
771 fixed with 4% paraformaldehyde (PFA) for 15 min at room temperature. After
772 washing with 1X PBS cells were analysed using FACS Verse flow cytometer
773 (BD Biosciences). The biosensor response was measured by analysing the
774 ratio upon excitation at 405 and 488 nm and emission at 510nm. Data was
775 analysed using FACSuite software. For each experiment the minimal and
776 maximal fluorescence ratios were determined, which correspond to 100%

777 sensor reduction and 100% sensor oxidation, respectively. Cumene
778 hydroperoxide (CHP, 0.5 mM) was used as the oxidant and dithiothreitol
779 (DTT, 40 mM) as the reductant. E_{GSH} was measured using the Nernst
780 equation as described previously [20].

781

782 **Co-cultures of U937 macrophages with J-Lat and U1 cells**

783 Co-cultures were performed according to earlier established protocol
784 [89]. U937 cells were seeded at a density of 0.2 million/ml in 24 well plates
785 and were infected with *Mtb* as described earlier. J-Lat and U1 cells were
786 added at a density of 0.1 million/ml on uninfected or infected U937
787 monolayers after amikacin treatment. Co-cultures were performed in complete
788 medium (RPMI 1640 plus 10% FCS, 2 mM L-glutamine) at 37 °C and 5% CO₂
789 for 5 days (d) in case of J-Lat cells and 48 h in case of U1 cells. Fresh media
790 was added in J-Lat cells after 48 h. At indicated time points, the supernatants
791 containing J-Lat and U1 cells were collected and centrifuged at 1500 rpm, 5
792 min to harvest cells. J-Lat and U1 cells were fixed in 4% PFA for 15 minutes,
793 centrifuged at 1500 rpm, 5 min and resuspended in 1X PBS for FACS
794 analysis. PMA and TNF- α were used at a final concentration of 5 ng/ml and
795 10 ng/ml, respectively.

796

797 **Culturing of J-Lat and U1 cells in U937-conditioned media**

798 J-Lat and U1 cells were seeded at a density of 0.1 million/ml in 24 well
799 plates in the absence or presence of two-fold dilutions of the supernatants
800 derived from *Mtb* uninfected or infected U937 macrophages. J-Lat and U1
801 cells were also cultured in two-fold dilution of the culture supernatant collected

802 from *Mtb* infected U937 macrophages grown in presence of 10 μ M of
803 exosome secretion inhibitor (GW4869). Presence of intact *Mtb* cells in the
804 supernatant was ruled out by passing of supernatant through 0.2 μ m filter
805 followed by confirmation of bacterial viability by plating of the supernatant. J-
806 Lat and U1 cells were harvested at different time points and were fixed in 4%
807 PFA for 15 minutes. After centrifugation cells were resuspended in 1X PBS for
808 FACS analysis.

809

810 **HIV-1 p24 staining**

811 For intracellular p24 staining, U1 cells were washed with FACS buffer
812 (1X PBS containing 10% human serum) followed by fixation and
813 permeabilization using the fixation/permeabilization kit (eBiosciences).
814 Permeabilized cells were then incubated with 100 μ l of 1:100 dilution of
815 phycoerythrin-conjugated mouse anti-p24 mAb (KC57-RD1; Beckman
816 Coulter, Inc.) for 30 min at 4 $^{\circ}$ C with intermittent mixing. After washing
817 samples twice with FACS buffer, cells were analysed with BD FACS Verse
818 Flow cytometer (BD Biosciences). Data was analysed using FACSuite
819 software.

820

821 **qRT-PCR**

822 Total RNA was isolated using RNeasy mini kit (Qiagen), according to
823 the manufacturer's instructions. RNA (500 ng) was reverse transcribed to
824 cDNA using iScriptTM cDNA synthesis kit (Bio-Rad) using random
825 oligonucleotide primers. p24 specific primers (p24, Forward- 5'
826 ATAATCCACCTATCCCAGTAGGAGAAAT 3' and Reverse- 5'

827 TTGGTTCCTTGTCTTATGTCCAGAATGC 3') were used to perform PCR.
828 Gene expression was analysed with real time PCR using iQTM SYBR Green
829 Supermix (Bio-Rad) and a CFX96 RT-PCR system (Bio-Rad). Data analysis
830 was performed with CFXManager™ software (Bio-Rad). The expression level
831 of each gene is normalized to human β -actin (Actin, Forward-
832 5'ATGTGGCCGAGGACTTTGATT 3' and Reverse- 5'
833 AGTGGGGTGGCTTTTAGGATG 3') gene.

834

835 **Isolation and purification of exosomes**

836 Exosomes were isolated and purified using ultrafiltration and exosome
837 precipitation technique as described previously [90, 91]. Briefly, ~60 million
838 RAW264.7 macrophages were cultured (6 million cells per 100 mm cell
839 culture dish) in cell culture dishes as described before [86] followed by
840 infection at moi 10 with *Mtb*, Hk-*Mtb*, Jal 1934 (MDR), MYC 431 (XDR) or left
841 uninfected. After infection, cells were washed thoroughly with 1X PBS and
842 incubated in serum free DMEM (Cell Clone) at 37 °C and 5% CO₂. Serum free
843 media was used cells to avoid contamination of exosomes present in the FBS
844 exosomes in the exosomes purified from macrophages infected with *Mtb*.
845 Culture supernatants were collected 24 h post infection (p.i.) and were
846 centrifuged at 5000 rpm for 15 min at 4 °C to remove cells, cell debris or any
847 *Mtb* in supernatant. Cleared culture supernatants were filtered twice through
848 0.22 μ m polyethersulphone (PES) filters (Jet Biofil™). Exosomes are 30-100
849 nm in diameter and filter freely through 0.22 μ m filters. Filtered supernatants
850 were concentrated to 1 ml using an Amicon Ultra-15 (Merck) with a 100 kDa
851 molecular weight cut off (MWCO) in a swing-out rotor (Thermo scientific™ SL

852 16) at 4 °C and 4000 × g. An equal volume of ExoQuick (Systems
853 BioSciences Inc. CA), exosome precipitation solution, was added to
854 concentrated culture supernatant, and the resulting solution was mixed by
855 inverting the tube and allowing it to stand overnight at 4 °C. This mixture was
856 then centrifuged at 1500 × g for 30 min. The supernatant was discarded, and
857 the precipitate consisted of exosomes was then re-suspended in sterile 1 ×
858 PBS (filtered through 0.22 µm filter) mixed with protease inhibitor cocktail
859 (Pierce™ Thermo Fisher Scientific) and were stored at -80 °C for future
860 analysis.

861

862 **Mouse infection and isolation of exosomes from serum and lungs**

863 6 to 8 week old BALB/c mice were infected with *Mtb* by aerosol with
864 ~100 bacilli per mouse or left uninfected as described previously [92]. At 20
865 weeks p.i., animals were sacrificed and serum and lungs were collected.
866 Exosomes were isolated from mouse serum by precipitating in ExoQuick
867 solution overnight as per manufacturer's instruction.

868

869 To isolate exosomes from lungs, 2ml of tissue digestion mix (Serum
870 free RPMI with 200 µg/ml Liberase DL [Sigma-Aldrich] and 100 µg/ml of
871 DNase [Thermo Fisher scientific]) was added to one whole lung and
872 transferred to C-tubes. Lungs were homogenised on gentleMACS™
873 Dissociator (Miltenyi Biotec) using machine program m_lung_01. Samples
874 were incubated for 30 min at 37 °C, 70-100 rpm followed by further
875 homogenizing lungs using machine program m_lung_02 for 22 sec. Lung
876 homogenates were passed through 40 µm cell strainer and centrifuged at

877 1500 rpm for 5 min. Supernatants were collected and passed through 0.22 μ m
878 filter. Filtered supernatants were concentrated to 1 mL and exosomes were
879 isolated using ExoQuick precipitation solution as described in above section.
880 Exosomes were stored in -80 °C for future analysis.

881

882 **Western blotting**

883 Exosome were lysed in RIPA buffer (25mM tris-HCl pH 7.6, 150 mM
884 NaCl, 1% NP-40, 1% sodium deoxycholate and 0.1% SDS) with protease
885 inhibitor (PierceTM Thermo Scientific). Protein estimation was performed using
886 micro BCA assay (PierceTM Thermo Fisher Scientific). 50 μ g of protein unless
887 specified was mixed with Laemmli buffer, heated at 95 °C for 5 min followed
888 by chilling on ice for 5 min before loading onto SDS-PAGE gel. Western
889 blotting was performed using LAMP2 (ab25631), Rab5b (BD-610281), Alix
890 (CST-2171), CD63 (sc-15363), p24 (ab9071), α -Tubulin (CST-2144) as
891 primary antibodies and goat anti-Rabbit IgG HRP (CST-7074) and horse anti-
892 mouse IgG (CST-7076) were used as secondary antibodies.

893

894 **Transmission electron microscopy**

895 Exosomes were fixed in 4% PFA for 10 min and 10 μ l sample was
896 mounted onto a carbon formvar coated copper grid. The samples were
897 allowed to adsorb on grids for 10 min to form a monolayer and the remaining
898 sample was wiped off using a clean filter paper. Grids were washed thrice
899 with 1X PBS followed by incubation in 50 μ l drop of 1% glutaraldehyde for 5
900 min. Grids were washed thoroughly with 1X PBS and stained with 2 μ l of

901 filtered 2% uranyl acetate solution for 1 min. After washing thrice with 1X PBS
902 grids were dried at room temperature.

903

904 For immunogold labelling of exosomes with anti-CD63 antibody,
905 exosomes were fixed in 4% PFA. Fixed exosome samples were mounted on
906 carbon formvar coated 300 mesh copper grids for 10 min before wiping
907 excess using filter paper. Grids were blocked in 0.5% bovine serum albumin
908 (BSA) in 1X PBS (blocking buffer) for 30 min and washed thrice in 1X PBS.
909 After this, grids were incubated in blocking buffer (negative control) or primary
910 antibody (CD63) diluted to 1:100 for 1 h. Grids were washed thoroughly with
911 1X PBS followed by incubation with anti-rabbit 10 nm gold antibody (ab27234)
912 diluted to 1:250 for 1h. Grids were then incubated in 1% glutaraldehyde for 5
913 min to fix the immunoreaction. Negative staining was performed using 2%
914 aqueous uranyl acetate solution for 1 min. After washing grids were air dried
915 and viewed with JEM 1011 transmission electron microscope at 120kV.

916

917 **NanoString gene array**

918 U1 cells were treated with 100 µg/ml concentration of exosomes for 12
919 h and total RNA was isolated using RNeasy mini kit (Qiagen) according to the
920 manufacturer's instructions. RNA concentration and purity were measured
921 using a Nanodrop Spectrophotometer (Thermo Fisher Scientific, Waltham,
922 MA). nCounter Gene Expression Assay was performed according to the
923 manufacturer's protocol. The assay utilized a custom made NanoString
924 codeset designed to measure 185 transcripts which includes 6 putative
925 housekeeping transcripts (see table S1a). This custom-made panel includes

926 genes reported to change expression in response to HIV infection and
927 oxidative stress. The data was normalized to the average counts for all
928 housekeeping genes in each sample and analysed in nSolver software
929 (NanoString Technologies).

930

931 **OCR measurement**

932 Oxygen consumption rate (OCR) was measured at 37 °C using
933 Seahorse XFp extracellular flux analyser (Seahorse Bioscience). XF cell
934 culture microplate plates were coated with 10 µl of Cell-Tak (Sigma-Aldrich)
935 reagent according to the manufacturer's protocol. U1 cells were treated with
936 exosomes isolated from *Mtb*, Hk-*mtb* infected or uninfected RAW264.7
937 macrophages at 100 µg/ml concentration for 48 h. After 48 h U1 cells were
938 washed and seeded in Seahorse flux analyser microplate pre-coated with
939 Cell-Tak at density of 50000 cells per well to generate a confluent monolayer
940 of cells. Agilent seahorse XFp cell mito stress kit (Agilent Technologies) was
941 utilized to carry out mitochondrial respiration assay. Briefly, three OCR
942 measurements were performed in XF assay media without addition of any
943 inhibitor to measure basal respiration, followed by sequential exposure of cells
944 to oligomycin (1 µM), an ATP synthase inhibitor and three OCR
945 measurements to determine the ATP-linked OCR and proton leak. Then,
946 cyanide-4-[trifluoromethoxy]phenylhydrazine (FCCP; 0.25 µM), an Electron
947 transport chain (ETC) uncoupler was injected to determine the maximal
948 respiration and the spare respiratory capacity (SRC). Lastly, antimycin A and
949 rotenone (0.5 µM each) inhibitor of complex III and I; respectively, were
950 injected to completely shut down the ETC to determine non-mitochondrial

951 respiration. The Wave Desktop 2.6 Software from Agilent website
952 ([https://www.agilent.com/en/products/cell-analysis/software-download-for-](https://www.agilent.com/en/products/cell-analysis/software-download-for-wave-desktop)
953 [wave-desktop](https://www.agilent.com/en/products/cell-analysis/software-download-for-wave-desktop)) was used for the calculation of the parameters from
954 mitochondrial respiration assay. Data was normalized according to protocol
955 described previously [93].

956

957 **Proteomic analysis of exosomes by LC-MS/MS**

958

959 We extracted proteins from exosomes as described previously for the
960 immuno-blotting experiment. Protein samples (30 µg) were resolved on 10%
961 SDS-PAGE gel up to a distance of 3 cm and stained with Coomassie Brilliant
962 Blue R250. The lanes were cut into three equal size bands. These bands
963 were first reduced with 5mM Tris (2-carboxyethyl) phosphine hydrochloride
964 (TCEP; Sigma- Aldrich) followed by alkylation with 50 mM iodoacetamide and
965 digested with 1µg trypsin for as long as 16 hours at 37 °C. The digests were
966 then cleaned up using C18 silica cartridge (The Nest Group, Southborough,
967 MA) and dried using speed vac which then was resuspended in Buffer A (5 %
968 acetonitrile / 0.1 % formic acid).

969

970 EASY-nLC 1000 system (Thermo Fisher Scientific) was used to
971 perform LC-MS/MS, coupled to QExactive mass spectrometer (Thermo Fisher
972 Scientific) fitted with nanoelectrospray ion source. 15cm Pico-Frit filled with
973 1.8 µm of C18 resin (Dr. Maeisch) was used to load and resolve 1 µg of the
974 peptide mixture with Buffer A. Loading and elution with 0-40% gradient of
975 Buffer B (95% acetonitrile/0.1% Formic acid) was given a flow rate of 300
976 nl/min and RT of 105 minutes. The MS was driven with a full scan resolution

977 of 70,000 at m/z of 400 and the MS/MS scans were acquired at a resolution of
978 17,500 at m/z of 400 using Top10 HCD Data-dependant acquisition mode.
979 Polydimethylcyclosiloxane (PCM) ions (m/z = 445.120025) was set up as lock
980 mass option for internal recalibration during the run. MS Data acquisition
981 was carried out using a Data-dependent Top10 method, which effectively
982 chooses most abundant precursor ions from a survey scan.

983

984 Raw files were analyzed using Thermo Proteome Discoverer 2.2
985 searched against Uniprot Mus musculus reference proteome database with
986 both PSM (peptide spectrum matches) and protein FDR set to 0.01 using
987 percolator node. For Sequest HT search, the precursor and fragment mass
988 tolerances were set at 10 ppm and 0.5 Da, respectively. Protein quantification
989 was done using Minora feature detector node with default settings and
990 considering only high PSM (peptide spectrum matches) confidence.

991

992 **Data processing and analysis**

993 Differential analysis was performed on Label-free quantification data
994 using R packages- ProstaR and DAPAR. The intensity values were log-
995 transformed followed by filtering of rows containing $NA \geq 5$ in the data.
996 Imputation was performed using R package-Mice. Limma-moderated t-test
997 was used to identify differentially expressed proteins and p values were
998 adjusted using BH method, between two groups. All proteins with fold change
999 >2 or <-2 and with $pvalue < 0.01$ were considered significant. Functional
1000 classification of differentially expressed proteins with GO and KEGG signalling
1001 pathway between two groups were analyzed using R package-clusterProfiler.

1002

1003 **Statistical analysis**

1004 Statistical analyses were performed using the GraphPad Prism
1005 software. Statistical analyses were performed using Student's *t*-tests (two-
1006 tailed). Comparisons of multiple groups were made by either using one-way or
1007 two-way ANOVA with Bonferroni multiple comparisons. Differences with
1008 a *p* value of < 0.05 were considered significant.

1009

1010 **Ethics statement**

1011 This study was carried out in strict accordance with the guidelines
1012 provided by the Committee for the Purpose of Control and Supervision on
1013 Experiments on Animals (CPCSEA), Government of India. The protocol was
1014 approved by the Animal Ethics Committee (AEC) of Indian Institute of Science
1015 (#CAF/Ethics/485/2016).

1016

1017 **Acknowledgments**

1018 This work was supported by the Wellcome trust-DBT India Alliance
1019 grant IA/S/16/2/502700 (AS), and in part by Department of Biotechnology
1020 (DBT) Grant BT/PR11911/BRB/10/1327/2014, BT/PR13522/COE/34/27/2015
1021 (AS), DBT-IISc Partnership Program (22-0905-0006-05- 987 436) and Infosys
1022 foundation. AS is a senior fellow of Wellcome trust-DBT India Alliance. PT and
1023 VKP acknowledge fellowships from CSIR and IISc, respectively.

1024

1025

1026

1027

1028

1029 **References**

- 1030 1. Whalen, C., et al., *Accelerated course of human immunodeficiency virus*
1031 *infection after tuberculosis*. Am J Respir Crit Care Med, 1995. **151**(1): p.
1032 129-35.
- 1033 2. Kwan, C.K. and J.D. Ernst, *HIV and tuberculosis: a deadly human syndemic*.
1034 Clin Microbiol Rev, 2011. **24**(2): p. 351-76.
- 1035 3. DeRiemer, K., et al., *Quantitative impact of human immunodeficiency virus*
1036 *infection on tuberculosis dynamics*. Am J Respir Crit Care Med, 2007.
1037 **176**(9): p. 936-44.
- 1038 4. Nusbaum, R.J., et al., *Pulmonary Tuberculosis in Humanized Mice Infected*
1039 *with HIV-1*. Sci Rep, 2016. **6**: p. 21522.
- 1040 5. Mwandumba, H.C., et al., *Mycobacterium tuberculosis resides in*
1041 *nonacidified vacuoles in endocytically competent alveolar macrophages*
1042 *from patients with tuberculosis and HIV infection*. J Immunol, 2004.
1043 **172**(7): p. 4592-8.
- 1044 6. Kalsdorf, B., et al., *HIV-1 infection impairs the bronchoalveolar T-cell*
1045 *response to mycobacteria*. Am J Respir Crit Care Med, 2009. **180**(12): p.
1046 1262-70.
- 1047 7. Diedrich, C.R. and J.L. Flynn, *HIV-1/mycobacterium tuberculosis coinfection*
1048 *immunology: how does HIV-1 exacerbate tuberculosis?* Infect Immun, 2011.
1049 **79**(4): p. 1407-17.
- 1050 8. Bafica, A., et al., *Cutting edge: in vivo induction of integrated HIV-1*
1051 *expression by mycobacteria is critically dependent on Toll-like receptor 2*. J
1052 Immunol, 2003. **171**(3): p. 1123-7.
- 1053 9. Toossi, Z., et al., *Increased replication of HIV-1 at sites of Mycobacterium*
1054 *tuberculosis infection: potential mechanisms of viral activation*. J Acquir
1055 Immune Defic Syndr, 2001. **28**(1): p. 1-8.
- 1056 10. Lederman, M.M., et al., *Mycobacterium tuberculosis and its purified protein*
1057 *derivative activate expression of the human immunodeficiency virus*. J
1058 Acquir Immune Defic Syndr, 1994. **7**(7): p. 727-33.
- 1059 11. Zhang, Y., et al., *Mycobacterium tuberculosis enhances human*
1060 *immunodeficiency virus-1 replication by transcriptional activation at the*
1061 *long terminal repeat*. J Clin Invest, 1995. **95**(5): p. 2324-31.
- 1062 12. Bernier, R., et al., *Mycobacterium tuberculosis mannose-capped*
1063 *lipoarabinomannan can induce NF-kappaB-dependent activation of human*
1064 *immunodeficiency virus type 1 long terminal repeat in T cells*. J Gen Virol,
1065 1998. **79 (Pt 6)**: p. 1353-61.
- 1066 13. Souriant, S., et al., *Tuberculosis Exacerbates HIV-1 Infection through IL-*
1067 *10/STAT3-Dependent Tunneling Nanotube Formation in Macrophages*. Cell
1068 Rep, 2019. **26**(13): p. 3586-3599 e7.
- 1069 14. Goletti, D., et al., *Inhibition of HIV-1 replication in monocyte-derived*
1070 *macrophages by Mycobacterium tuberculosis*. J Infect Dis, 2004. **189**(4): p.
1071 624-33.
- 1072 15. Ranjbar, S., et al., *HIV-1 replication is differentially regulated by distinct*
1073 *clinical strains of Mycobacterium tuberculosis*. PLoS One, 2009. **4**(7): p.
1074 e6116.

- 1075 16. Perl, A. and K. Banki, *Genetic and metabolic control of the mitochondrial*
1076 *transmembrane potential and reactive oxygen intermediate production in*
1077 *HIV disease*. *Antioxid Redox Signal*, 2000. **2**(3): p. 551-73.
- 1078 17. Herzenberg, L.A., et al., *Glutathione deficiency is associated with impaired*
1079 *survival in HIV disease*. *Proc Natl Acad Sci U S A*, 1997. **94**(5): p. 1967-72.
- 1080 18. Peterson, J.D., et al., *Glutathione levels in antigen-presenting cells modulate*
1081 *Th1 versus Th2 response patterns*. *Proc Natl Acad Sci U S A*, 1998. **95**(6): p.
1082 3071-6.
- 1083 19. De Rosa, S.C., et al., *N-acetylcysteine replenishes glutathione in HIV*
1084 *infection*. *Eur J Clin Invest*, 2000. **30**(10): p. 915-29.
- 1085 20. Bhaskar, A., et al., *Measuring glutathione redox potential of HIV-1-infected*
1086 *macrophages*. *J Biol Chem*, 2015. **290**(2): p. 1020-38.
- 1087 21. Guerra, C., et al., *Glutathione and adaptive immune responses against*
1088 *Mycobacterium tuberculosis infection in healthy and HIV infected*
1089 *individuals*. *PLoS One*, 2011. **6**(12): p. e28378.
- 1090 22. Palanisamy, G.S., et al., *Evidence for oxidative stress and defective*
1091 *antioxidant response in guinea pigs with tuberculosis*. *PLoS One*, 2011.
1092 **6**(10): p. e26254.
- 1093 23. Cumming, B.M., et al., *Mycobacterium tuberculosis induces decelerated*
1094 *bioenergetic metabolism in human macrophages*. *Elife*, 2018. **7**.
- 1095 24. Gutscher, M., et al., *Real-time imaging of the intracellular glutathione redox*
1096 *potential*. *Nat Methods*, 2008. **5**(6): p. 553-9.
- 1097 25. Choi, H.H., et al., *Endoplasmic reticulum stress response is involved in*
1098 *Mycobacterium tuberculosis protein ESAT-6-mediated apoptosis*. *FEBS Lett*,
1099 **584**(11): p. 2445-54.
- 1100 26. Shenoi, S., et al., *Multidrug-resistant and extensively drug-resistant*
1101 *tuberculosis: consequences for the global HIV community*. *Curr Opin Infect*
1102 *Dis*, 2009. **22**(1): p. 11-7.
- 1103 27. Wells, C.D., et al., *HIV infection and multidrug-resistant tuberculosis: the*
1104 *perfect storm*. *J Infect Dis*, 2007. **196** **Suppl 1**: p. S86-107.
- 1105 28. Kumar, D., et al., *Genome-wide analysis of the host intracellular network*
1106 *that regulates survival of Mycobacterium tuberculosis*. *Cell*, 2010. **140**(5):
1107 p. 731-43.
- 1108 29. Jordan, A., D. Bisgrove, and E. Verdin, *HIV reproducibly establishes a latent*
1109 *infection after acute infection of T cells in vitro*. *EMBO J*, 2003. **22**(8): p.
1110 1868-77.
- 1111 30. Folks, T.M., et al., *Cytokine-induced expression of HIV-1 in a chronically*
1112 *infected promonocyte cell line*. *Science*, 1987. **238**(4828): p. 800-2.
- 1113 31. Poli, G., et al., *Tumor necrosis factor alpha functions in an autocrine manner*
1114 *in the induction of human immunodeficiency virus expression*. *Proc Natl*
1115 *Acad Sci U S A*, 1990. **87**(2): p. 782-5.
- 1116 32. Kurosaka, K., N. Watanabe, and Y. Kobayashi, *Production of*
1117 *proinflammatory cytokines by phorbol myristate acetate-treated THP-1*
1118 *cells and monocyte-derived macrophages after phagocytosis of apoptotic*
1119 *CTLL-2 cells*. *J Immunol*, 1998. **161**(11): p. 6245-9.
- 1120 33. Bhatnagar, S., et al., *Exosomes released from macrophages infected with*
1121 *intracellular pathogens stimulate a proinflammatory response in vitro and*
1122 *in vivo*. *Blood*, 2007. **110**(9): p. 3234-44.

- 1123 34. Chan, J.K. and W.C. Greene, *NF-kappaB/Rel: agonist and antagonist roles in*
1124 *HIV-1 latency*. *Curr Opin HIV AIDS*, 2011. **6**(1): p. 12-8.
- 1125 35. Essandoh, K., et al., *Blockade of exosome generation with GW4869 dampens*
1126 *the sepsis-induced inflammation and cardiac dysfunction*. *Biochim Biophys*
1127 *Acta*, 2015. **1852**(11): p. 2362-71.
- 1128 36. Perez, V.L., et al., *An HIV-1-infected T cell clone defective in IL-2 production*
1129 *and Ca²⁺ mobilization after CD3 stimulation*. *J Immunol*, 1991. **147**(9): p.
1130 3145-8.
- 1131 37. Singh, P.P., et al., *Exosomes isolated from mycobacteria-infected mice or*
1132 *cultured macrophages can recruit and activate immune cells in vitro and in*
1133 *vivo*. *J Immunol*, 2012. **189**(2): p. 777-85.
- 1134 38. Booth, A.M., et al., *Exosomes and HIV Gag bud from endosome-like domains*
1135 *of the T cell plasma membrane*. *J Cell Biol*, 2006. **172**(6): p. 923-35.
- 1136 39. Lee, Y., S. El Andaloussi, and M.J. Wood, *Exosomes and microvesicles:*
1137 *extracellular vesicles for genetic information transfer and gene therapy*.
1138 *Hum Mol Genet*, 2012. **21**(R1): p. R125-34.
- 1139 40. Staal, F.J., et al., *Intracellular thiols regulate activation of nuclear factor*
1140 *kappa B and transcription of human immunodeficiency virus*. *Proc Natl*
1141 *Acad Sci U S A*, 1990. **87**(24): p. 9943-7.
- 1142 41. Pyo, C.W., et al., *Reactive oxygen species activate HIV long terminal repeat*
1143 *via post-translational control of NF-kappaB*. *Biochem Biophys Res*
1144 *Commun*, 2008. **376**(1): p. 180-5.
- 1145 42. Kulkarni, M.M., *Digital multiplexed gene expression analysis using the*
1146 *NanoString nCounter system*. *Curr Protoc Mol Biol*, 2011. **Chapter 25**: p.
1147 Unit25B 10.
- 1148 43. Salzano, S., et al., *Linkage of inflammation and oxidative stress via release of*
1149 *glutathionylated peroxiredoxin-2, which acts as a danger signal*. *Proc Natl*
1150 *Acad Sci U S A*, 2014. **111**(33): p. 12157-62.
- 1151 44. Volonte, D. and F. Galbiati, *Inhibition of thioredoxin reductase 1 by caveolin*
1152 *1 promotes stress-induced premature senescence*. *EMBO Rep*, 2009.
1153 **10**(12): p. 1334-40.
- 1154 45. Yang, X., et al., *Mn Inhibits GSH Synthesis via Downregulation of Neuronal*
1155 *EAAC1 and Astrocytic xCT to Cause Oxidative Damage in the Striatum of*
1156 *Mice*. *Oxid Med Cell Longev*, 2018. **2018**: p. 4235695.
- 1157 46. Lee, J.H., et al., *Ferritin binds and activates p53 under oxidative stress*.
1158 *Biochem Biophys Res Commun*, 2009. **389**(3): p. 399-404.
- 1159 47. Gill, A.J., et al., *Heme oxygenase-1 promoter region (GT)_n polymorphism*
1160 *associates with increased neuroimmune activation and risk for encephalitis*
1161 *in HIV infection*. *J Neuroinflammation*, 2018. **15**(1): p. 70.
- 1162 48. Gao, Y., et al., *Activation of the selenoprotein SEPS1 gene expression by pro-*
1163 *inflammatory cytokines in HepG2 cells*. *Cytokine*, 2006. **33**(5): p. 246-51.
- 1164 49. Nakamura, K., et al., *PB1 domain interaction of p62/sequestosome 1 and*
1165 *MEKK3 regulates NF-kappaB activation*. *J Biol Chem*, 2010. **285**(3): p.
1166 2077-89.
- 1167 50. Roebuck, K.A., D.S. Gu, and M.F. Kagnoff, *Activating protein-1 cooperates*
1168 *with phorbol ester activation signals to increase HIV-1 expression*. *AIDS*,
1169 1996. **10**(8): p. 819-26.
- 1170 51. Mamik, M.K. and A. Ghorpade, *Chemokine CXCL8 promotes HIV-1*
1171 *replication in human monocyte-derived macrophages and primary*

- 1172 *microglia via nuclear factor-kappaB pathway*. PLoS One, 2014. **9**(3): p.
1173 e92145.
- 1174 52. Ansari, A.W., A. Kamarulzaman, and R.E. Schmidt, *Multifaceted Impact of*
1175 *Host C-C Chemokine CCL2 in the Immuno-Pathogenesis of HIV-1/M.*
1176 *tuberculosis Co-Infection*. Front Immunol, 2013. **4**: p. 312.
- 1177 53. Albin, J.S. and R.S. Harris, *Interactions of host APOBEC3 restriction factors*
1178 *with HIV-1 in vivo: implications for therapeutics*. Expert Rev Mol Med,
1179 2010. **12**: p. e4.
- 1180 54. Sadler, H.A., et al., *APOBEC3G contributes to HIV-1 variation through*
1181 *sublethal mutagenesis*. J Virol, 2010. **84**(14): p. 7396-404.
- 1182 55. Toossi, Z., et al., *Short Communication: Expression of APOBEC3G and*
1183 *Interferon Gamma in Pleural Fluid Mononuclear Cells from HIV/TB Dual*
1184 *Infected Subjects*. AIDS Res Hum Retroviruses, 2015. **31**(7): p. 692-5.
- 1185 56. Santos, S., et al., *Virus-producing cells determine the host protein profiles of*
1186 *HIV-1 virion cores*. Retrovirology, 2012. **9**: p. 65.
- 1187 57. Hegedus, A., M. Kavanagh Williamson, and H. Huthoff, *HIV-1 pathogenicity*
1188 *and virion production are dependent on the metabolic phenotype of*
1189 *activated CD4+ T cells*. Retrovirology, 2014. **11**: p. 98.
- 1190 58. Chacko, B.K., et al., *The Bioenergetic Health Index: a new concept in*
1191 *mitochondrial translational research*. Clin Sci (Lond), 2014. **127**(6): p.
1192 367-73.
- 1193 59. Schorey, J.S., et al., *Exosomes and other extracellular vesicles in host-*
1194 *pathogen interactions*. EMBO Rep, 2015. **16**(1): p. 24-43.
- 1195 60. Cheng, Y. and J.S. Schorey, *Extracellular vesicles deliver Mycobacterium*
1196 *RNA to promote host immunity and bacterial killing*. EMBO Rep, 2019.
1197 **20**(3).
- 1198 61. Rottenberg, D.A., et al., *Abnormal cerebral glucose metabolism in HIV-1*
1199 *seropositive subjects with and without dementia*. J Nucl Med, 1996. **37**(7):
1200 p. 1133-41.
- 1201 62. Palmer, C.S., et al., *Glucose Metabolism in T Cells and Monocytes: New*
1202 *Perspectives in HIV Pathogenesis*. EBioMedicine, 2016. **6**: p. 31-41.
- 1203 63. Townsend, D.M., K.D. Tew, and H. Tapiero, *Sulfur containing amino acids*
1204 *and human disease*. Biomed Pharmacother, 2004. **58**(1): p. 47-55.
- 1205 64. Rao, S., et al., *Host mRNA decay proteins influence HIV-1 replication and*
1206 *viral gene expression in primary monocyte-derived macrophages*.
1207 Retrovirology, 2019. **16**(1): p. 3.
- 1208 65. Kok, Y.L., et al., *Spontaneous reactivation of latent HIV-1 promoters is*
1209 *linked to the cell cycle as revealed by a genetic-insulators-containing dual-*
1210 *fluorescence HIV-1-based vector*. Sci Rep, 2018. **8**(1): p. 10204.
- 1211 66. Felty, Q., et al., *Estrogen-induced mitochondrial reactive oxygen species as*
1212 *signal-transducing messengers*. Biochemistry, 2005. **44**(18): p. 6900-9.
- 1213 67. Das, B., et al., *Estrogen receptor-1 is a key regulator of HIV-1 latency that*
1214 *imparts gender-specific restrictions on the latent reservoir*. Proc Natl Acad
1215 Sci U S A, 2018. **115**(33): p. E7795-E7804.
- 1216 68. Duette, G., et al., *Induction of HIF-1alpha by HIV-1 Infection in CD4(+) T*
1217 *Cells Promotes Viral Replication and Drives Extracellular Vesicle-Mediated*
1218 *Inflammation*. MBio, 2018. **9**(5).
- 1219 69. Anand, P.K., et al., *Exosomal Hsp70 induces a pro-inflammatory response to*
1220 *foreign particles including mycobacteria*. PLoS One, 2010. **5**(4): p. e10136.

- 1221 70. Anderson, I., et al., *Heat shock protein 90 controls HIV-1 reactivation from*
1222 *latency*. Proc Natl Acad Sci U S A, 2014. **111**(15): p. E1528-37.
- 1223 71. Abdel-Mohsen, M., et al., *Human Galectin-9 Is a Potent Mediator of HIV*
1224 *Transcription and Reactivation*. PLoS Pathog, 2016. **12**(6): p. e1005677.
- 1225 72. Aalinkeel, R., et al., *Galectin-1 Reduces Neuroinflammation via Modulation*
1226 *of Nitric Oxide-Arginase Signaling in HIV-1 Transfected Microglia: a Gold*
1227 *Nanoparticle-Galectin-1 "Nanoplex" a Possible Neurotherapeutic?* J
1228 Neuroimmune Pharmacol, 2017. **12**(1): p. 133-151.
- 1229 73. Chaudhuri, A., et al., *STAT1 signaling modulates HIV-1-induced*
1230 *inflammatory responses and leukocyte transmigration across the blood-*
1231 *brain barrier*. Blood, 2008. **111**(4): p. 2062-72.
- 1232 74. Tjernlund, A., et al., *Leukemia inhibitor factor (LIF) inhibits HIV-1*
1233 *replication via restriction of stat 3 activation*. AIDS Res Hum Retroviruses,
1234 2007. **23**(3): p. 398-406.
- 1235 75. Barondes, S.H., et al., *Galectins: a family of animal beta-galactoside-binding*
1236 *lectins*. Cell, 1994. **76**(4): p. 597-8.
- 1237 76. Alvarez-Jimenez, V.D., et al., *Extracellular Vesicles Released from*
1238 *Mycobacterium tuberculosis-Infected Neutrophils Promote Macrophage*
1239 *Autophagy and Decrease Intracellular Mycobacterial Survival*. Front
1240 Immunol, 2018. **9**: p. 272.
- 1241 77. Murphy, M.P., *How mitochondria produce reactive oxygen species*. Biochem
1242 J, 2009. **417**(1): p. 1-13.
- 1243 78. Vilhardt, F., et al., *The HIV-1 Nef protein and phagocyte NADPH oxidase*
1244 *activation*. J Biol Chem, 2002. **277**(44): p. 42136-43.
- 1245 79. Kim, C., J.Y. Kim, and J.H. Kim, *Cytosolic phospholipase A(2), lipoxygenase*
1246 *metabolites, and reactive oxygen species*. BMB Rep, 2008. **41**(8): p. 555-9.
- 1247 80. Coffey, M.J., et al., *Granulocyte-macrophage colony-stimulating factor*
1248 *upregulates reduced 5-lipoxygenase metabolism in peripheral blood*
1249 *monocytes and neutrophils in acquired immunodeficiency syndrome*. Blood,
1250 1999. **94**(11): p. 3897-905.
- 1251 81. Chen, C., et al., *Identification of a Novel Serum Biomarker for Tuberculosis*
1252 *Infection in Chinese HIV Patients by iTRAQ-Based Quantitative Proteomics*.
1253 Front Microbiol, 2018. **9**: p. 330.
- 1254 82. Banfer, S., et al., *Molecular mechanism to recruit galectin-3 into*
1255 *multivesicular bodies for polarized exosomal secretion*. Proc Natl Acad Sci U
1256 S A, 2018. **115**(19): p. E4396-E4405.
- 1257 83. Fulton, D.J.R., et al., *Galectin-3: A Harbinger of Reactive Oxygen Species,*
1258 *Fibrosis, and Inflammation in Pulmonary Arterial Hypertension*. Antioxid
1259 Redox Signal, 2019.
- 1260 84. Zhao, J., et al., *Secretion of IFN-gamma Associated with Galectin-9*
1261 *Production by Pleural Fluid Cells from a Patient with Extrapulmonary*
1262 *Tuberculosis*. Int J Mol Sci, 2017. **18**(7).
- 1263 85. Infante, J.R., et al., *Phase I dose-escalation studies of SNX-5422, an orally*
1264 *bioavailable heat shock protein 90 inhibitor, in patients with refractory*
1265 *solid tumours*. Eur J Cancer, 2014. **50**(17): p. 2897-904.
- 1266 86. Bhaskar, A., et al., *Reengineering redox sensitive GFP to measure mycothiol*
1267 *redox potential of Mycobacterium tuberculosis during infection*. PLoS
1268 Pathog, 2014. **10**(1): p. e1003902.

- 1269 87. Srivastava, M., et al., *Mediator responses of alveolar macrophages and*
1270 *kinetics of mononuclear phagocyte subset recruitment during acute*
1271 *primary and secondary mycobacterial infections in the lungs of mice.* Cell
1272 Microbiol, 2007. **9**(3): p. 738-52.
- 1273 88. Malik, Z.A., G.M. Denning, and D.J. Kusner, *Inhibition of Ca(2+) signaling by*
1274 *Mycobacterium tuberculosis is associated with reduced phagosome-*
1275 *lysosome fusion and increased survival within human macrophages.* J Exp
1276 Med, 2000. **191**(2): p. 287-302.
- 1277 89. Borghi, M.O., et al., *Interaction between chronically HIV-infected*
1278 *promonocytic cells and human umbilical vein endothelial cells: role of*
1279 *proinflammatory cytokines and chemokines in viral expression modulation.*
1280 Clin Exp Immunol, 2000. **120**(1): p. 93-100.
- 1281 90. Zeringer, E., et al., *Strategies for isolation of exosomes.* Cold Spring Harb
1282 Protoc, 2015. **2015**(4): p. 319-23.
- 1283 91. Li, P., et al., *Progress in Exosome Isolation Techniques.* Theranostics, 2017.
1284 **7**(3): p. 789-804.
- 1285 92. Mishra, S., et al., *Efficacy of beta-lactam/beta-lactamase inhibitor*
1286 *combination is linked to WhiB4-mediated changes in redox physiology of*
1287 *Mycobacterium tuberculosis.* 2017. **6**.
- 1288 93. Yang, Y., et al., *Metabolic reprogramming for producing energy and*
1289 *reducing power in fumarate hydratase null cells from hereditary*
1290 *leiomyomatosis renal cell carcinoma.* PLoS One, 2013. **8**(8): p. e72179.
1291

1292

1293

1294

1295

1296

1297

1298

1299

1300

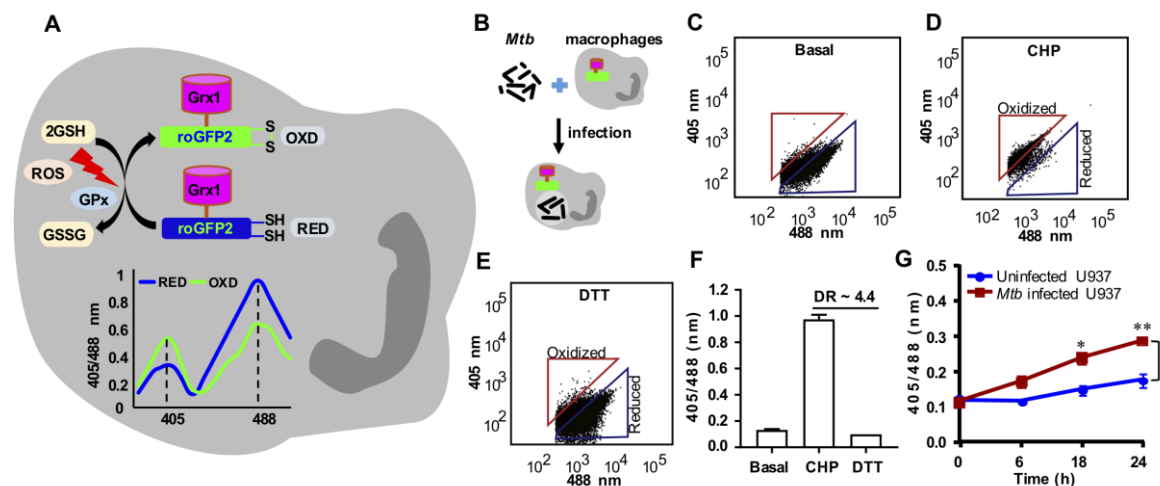
1301

1302

1303

1304

1305



1306

1307 **Fig. 1. *Mycobacterium tuberculosis* (*Mtb*) induces oxidative shift in E_{GSH}**

1308 **of U937 macrophages ($M\phi$). (A) Schematic representation of Grx1-roGFP2**

1309 **oxidation and reduction in response to ROS inside a mammalian cell stably**

1310 **expressing the biosensor. GPx denotes GSH-dependent glutathione**

1311 **peroxidase. The graph represents the 405/488 nm ratios change upon**

1312 **oxidation or reduction of Grx1-roGFP2 in response to oxidative or reductive**

1313 **stress. Oxidative stress increases fluorescence at 405 nm excitation and**

1314 **decreases fluorescence at 488 nm at a constant emission of 510 nm, whereas**

1315 **an opposite biosensor response is induced by reductive stress. (B) PMA**

1316 **differentiated U937 $M\phi$ stably expressing Grx1-roGFP2 in the cytosol were**

1317 **infected with *Mtb* H37Rv at a multiplicity of infection (MOI) 10. At the indicated**

1318 **time points, ratiometric sensor response was measured by exciting the sensor**

1319 **at 405 and 488 nm lasers and at a constant emission of 510 nm using flow**

1320 **cytometer. Dot plot spectra showing the ratiometric shift in the biosensor**

1321 **response in case of (C) untreated U937 (basal) and upon treatment of with**

1322 **(D) an oxidant cumene hydroperoxide (CHP, 0.5 mM) and (E) a reductant**

1323 **dithiothreitol (DTT, 40 mM). (F) Dynamic range (DR) of the biosensor in U937**

1324 **cells based on the complete oxidation and reduction by CHP and DTT,**

1325 respectively. **(G)** Ratiometric biosensor response over time in case of
1326 uninfected and *Mtb* infected U937 macrophages. Error bars represent
1327 standard deviations from the mean. * $p < 0.05$; ** $p < 0.01$ (two-way ANOVA).
1328 Data are representative of at least three independent experiments performed
1329 in triplicate.

1330

1331

1332

1333

1334

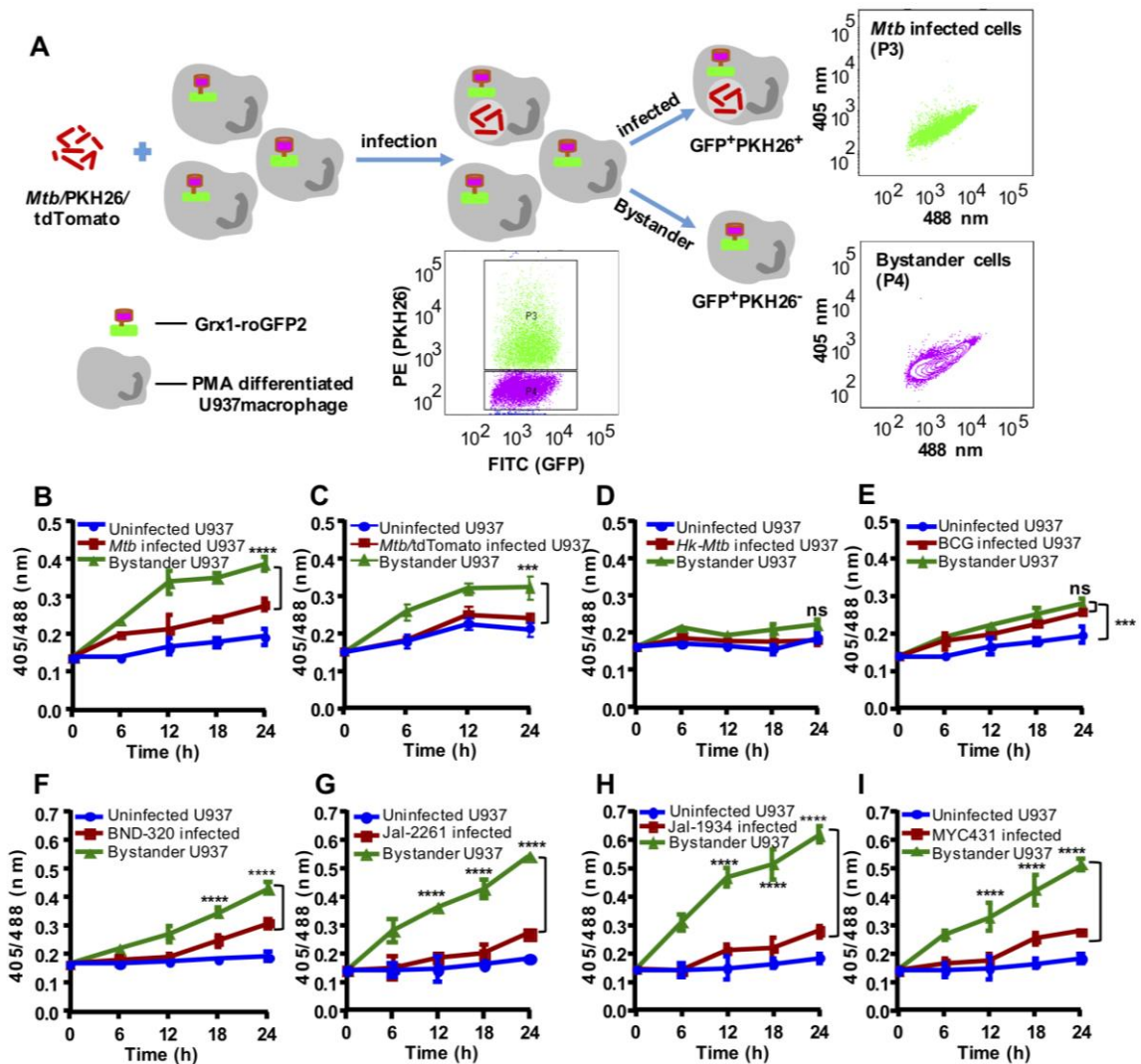
1335

1336

1337

1338

1339



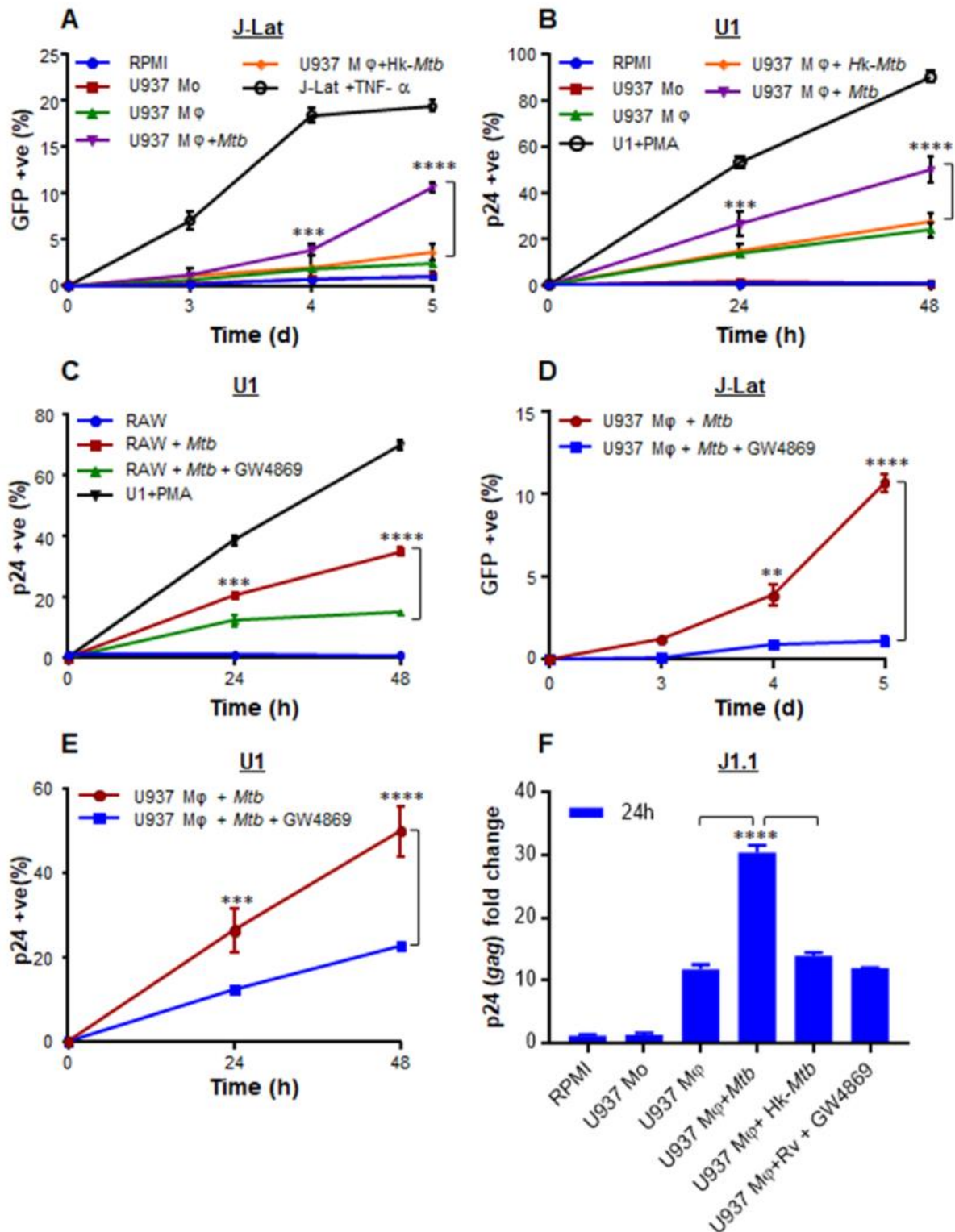
1340

1341 **Fig. 2. *Mycobacterium tuberculosis* (*Mtb*) induces higher oxidative shift**
 1342 **in E_{GSH} of bystander as compared to infected U937 macrophages ($M\phi$).**

1343 **(A)** The *Mtb* H37Rv bacilli were stained with a membrane staining dye PKH26
 1344 and PMA differentiated U937/Grx1-roGFP2 cells were infected at MOI 10. The
 1345 sensor response was measured by flow cytometry. Based on the PKH26
 1346 fluorescence emitted by *Mtb* inside $M\phi$, the U937/Grx1-roGFP2 $M\phi$ were
 1347 gated into infected (P3) or bystander subpopulations (P4) and the dot plot
 1348 spectra of *Mtb* infected and bystander U937/Grx1-roGFP2 at 24 h is shown.

1349 **(B)** The line graph showing biosensor response at various time points in case
 1350 of uninfected, *Mtb* infected, and bystander U937/Grx1-roGFP2. **(C)** *Mtb* stably

1351 expressing red fluorescent protein, tdTomato (*Mtb*/tdTomato) was used to
1352 infect U937/Grx1-roGFP2 (MOI 10) and the biosensor response of uninfected,
1353 infected and bystander cells was measured over time. Biosensor response of
1354 infected and bystander U937/Grx1-roGFP2 cells upon infection with *PKH-26*
1355 labeled **(D)** heat-killed *Mtb* (Hk-*Mtb*), **(E)** *M. bovis* BCG strain, drug resistant
1356 clinical isolates of *Mtb* **(F)** BND-320, **(G)** Jal-2261, **(H)** Jal-1934 and **(I)** MYC-
1357 431. Error bars represent standard deviations from the mean. *** $p < 0.001$; ****
1358 $p < 0.0001$ (two-way ANOVA). Data are representative of at least three
1359 independent experiments performed in triplicate.
1360



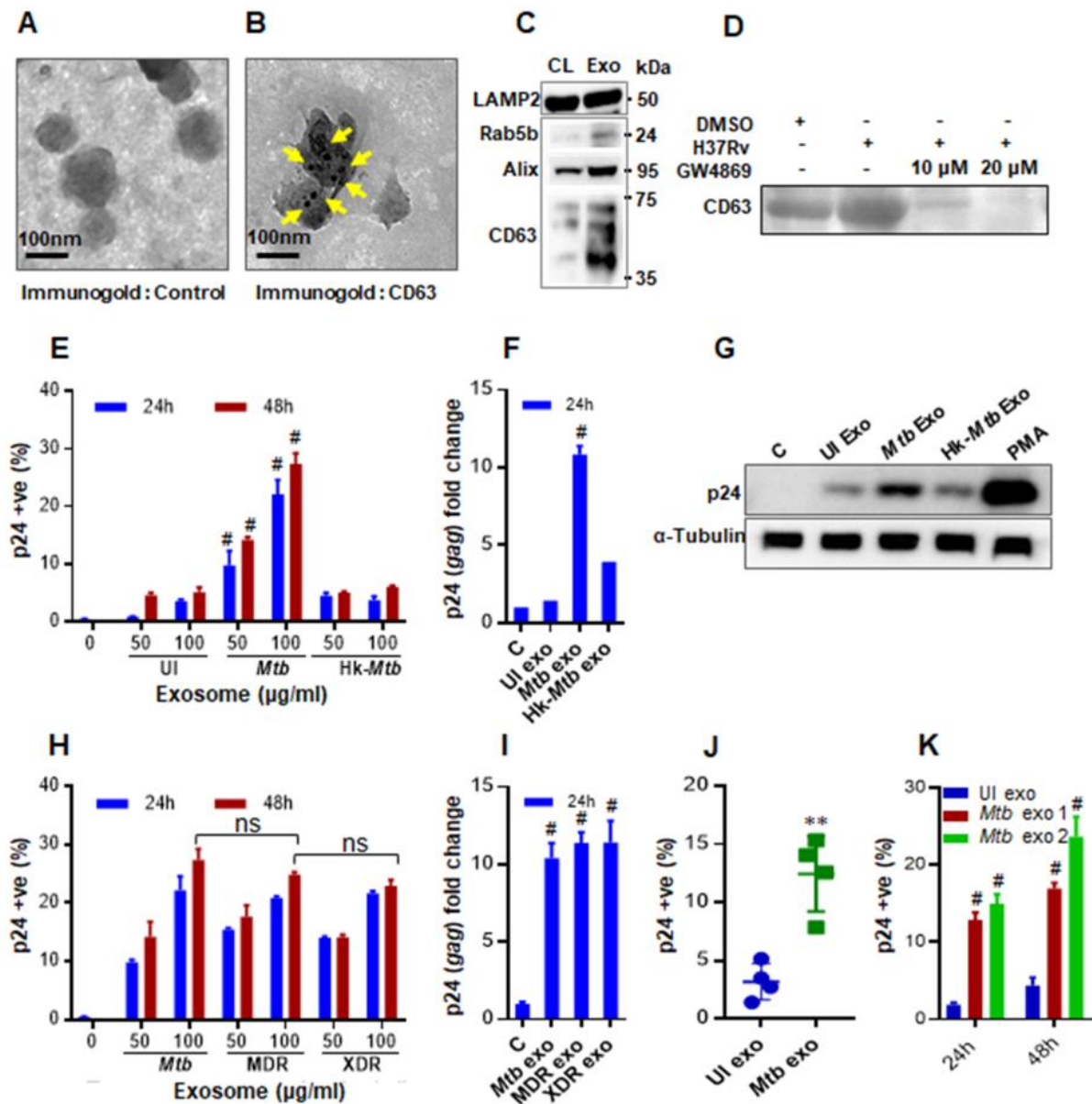
1361

1362 **Fig. 3. Culture supernatant derived from *Mtb* infected macrophages (Mφ)**

1363 **reactivates HIV-1.** We determined the influence of culture supernatant

1364 derived from *Mtb* infected Mφ on three latent cell lines of HIV-1: J-Lat, U1,

1365 and J1.1. The U937 M ϕ were infected with *Mtb* or Hk-*Mtb* (MOI 10). At 24 h
1366 p.i., culture supernatant from the infected macrophages was collected, passed
1367 through 0.2 μ m filter, and diluted in fresh RPMI medium (1:1, v/v). This
1368 supernatant was used to culture J-Lat and U1 cells and HIV-1 reactivation
1369 was monitored over time by measuring **(A)** GFP fluorescence in J-Lat and by
1370 **(B)** p24 immuno-staining in U1 cells. As controls, we similarly monitored HIV-
1371 1 reactivation from J-Lat and U1 cells, cultured in the supernatant derived
1372 from U937 monocytes (mo) and PMA-differentiated U937 M ϕ . HIV-1
1373 reactivation upon treatment of J-Lat and U1 with TNF α (10 ng/ml) and PMA (5
1374 ng/ml), respectively, was taken as positive control. **(C)** HIV-1 reactivation in
1375 U1 upon treatment with the supernatant derived from RAW264.7 M ϕ infected
1376 with *Mtb* for 24 h. Supernatant from uninfected RAW264.7 M ϕ and PMA-
1377 treatment were used as negative and positive controls for HIV-1 reactivation,
1378 respectively. To investigate if supernatant mediated HIV-1 reactivation is
1379 dependent on the presence of extracellular vesicles (e.g., exosomes), we
1380 treated *Mtb* infected U937 and RAW264.7 M ϕ with an inhibitor of exosome
1381 secretion (GW4869) for 24 h, followed by supernatant collection and
1382 reactivation of HIV-1 in U1 **(C and E)**, J-Lat **(D)**, and J1.1 **(F)** cells as
1383 described earlier. HIV-1 reactivation was measured by p24 (*gag*) qRT-PCR in
1384 J1.1 cells. Error bars represent standard deviations from the mean. ** p<0.01;
1385 *** p<0.001; ****p<0.0001. Data are representative of at least two
1386 independent experiments performed in triplicate.
1387
1388



1389

1390 **Fig. 4. Exosomes derived from *Mtb* infected macrophages (Mφ) and mice**

1391 **induce HIV reactivation.** Exosomes were isolated from enriched cell culture

1392 supernatant of *Mtb* infected RAW 264.7 Mφ. Exosomes were purified by using

1393 the ExoQuick precipitation solution and morphologically characterized by

1394 transmission electron microscopy (TEM). **(A)** Control, **(B)** Immunogold

1395 labeling of exosomes using the antibody against exosomes surface marker,

1396 CD63. Scale bar, 100 nm, **(C)** Immuno-blot analysis of LAMP2, Rab5b, Alix

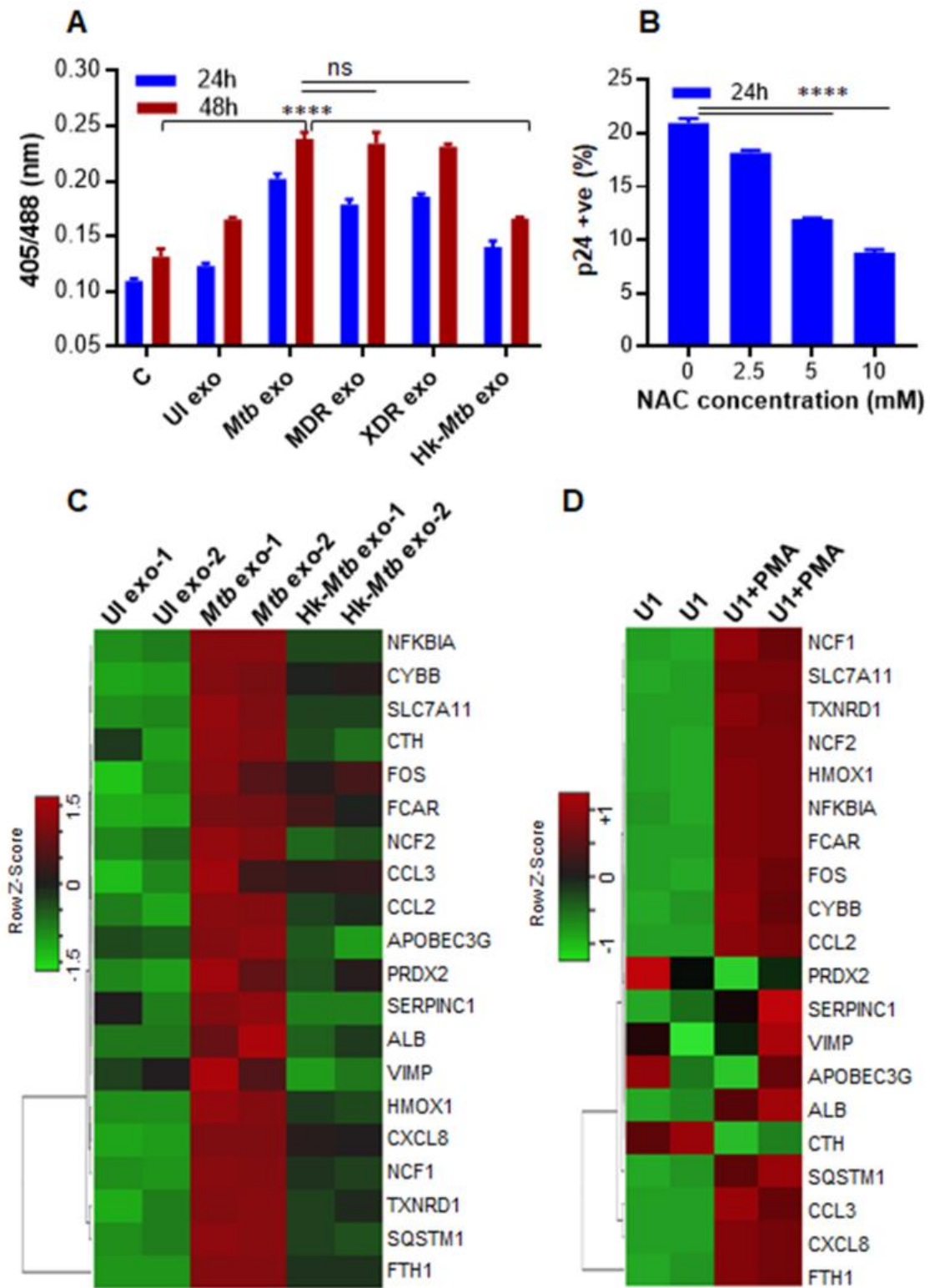
1397 and CD63 in cell extract (CL; 30 μg) and purified exosomes (Exo, 30 μg) from

1398 *Mtb* infected RAW264.7 M ϕ , **(D)** Immuno- blot analysis of exosome-specific
1399 marker CD63 to show dose dependent reduction in exosome production by
1400 *Mtb* infected RAW 264.7 M ϕ upon treatment with GW4869. Exosomes were
1401 derived from equal number of RAW 264.7 M ϕ in each case and equivalent
1402 volume was loaded in each lane. **(E)** U1 cells were treated with 50 and 100
1403 μ g/ml of purified exosomes and HIV-1 reactivation was measured by flow
1404 cytometry using PE labeled antibody specific to p24 (Gag) antigen at the
1405 indicated time-points, **(F)** qRT-PCR for *gag* transcript at 24 h post-treatment
1406 with 100 μ g/ml of purified exosomes, **(G)** immuno-blot for p24 in the cell lysate
1407 (50 μ g) at 24 h post-treatment with 100 μ g/ml of purified exosomes. CTR and
1408 UI exo denote HIV-1 reactivation without any treatment or upon treatment with
1409 exosomes (100 μ g/ml) derived from uninfected RAW 264.7 M ϕ , respectively.
1410 RAW264.7 M ϕ were infected with MDR (Jal-1934) and XDR (Myc431) strains
1411 for 24 h and exosomes were isolated. U1 cells were treated with exosomes
1412 and HIV-1 reactivation was monitored at the indicated time by flow cytometry
1413 using **(H)** PE labeled antibody specific to p24 (Gag) antigen and **(I)** qRT-PCR
1414 of *gag* transcript. BALB/c mice were infected with 100 CFU of *Mtb* H37Rv or
1415 were left uninfected. Exosomes were isolated from mouse serum and from the
1416 lung tissue at 20 weeks post infection using ExoQuick and quantified by micro
1417 BCA assay. U1 cells were treated with exosomes derived from **(J)** serum (2
1418 mg/ml) or **(K)** from lungs (*Mtb* exo1 - 100 μ g/ml, *Mtb* exo2 - 200 μ g/ml) and
1419 HIV reactivation was measured by flow cytometry using fluorescent tagged
1420 antibody (PE labeled) specific to p24 (Gag) antigen. Error bars represent
1421 standard deviations from the mean. Statistical analyses were performed using
1422 two tailed unpaired t-test **(J)**, one-way ANOVA **(F, I)** and two-way ANOVA **(E,**

1423 H, K). ns- non significant; **p<0.01; # p<0.001. Data are representative of at

1424 least two independent experiments performed in duplicate.

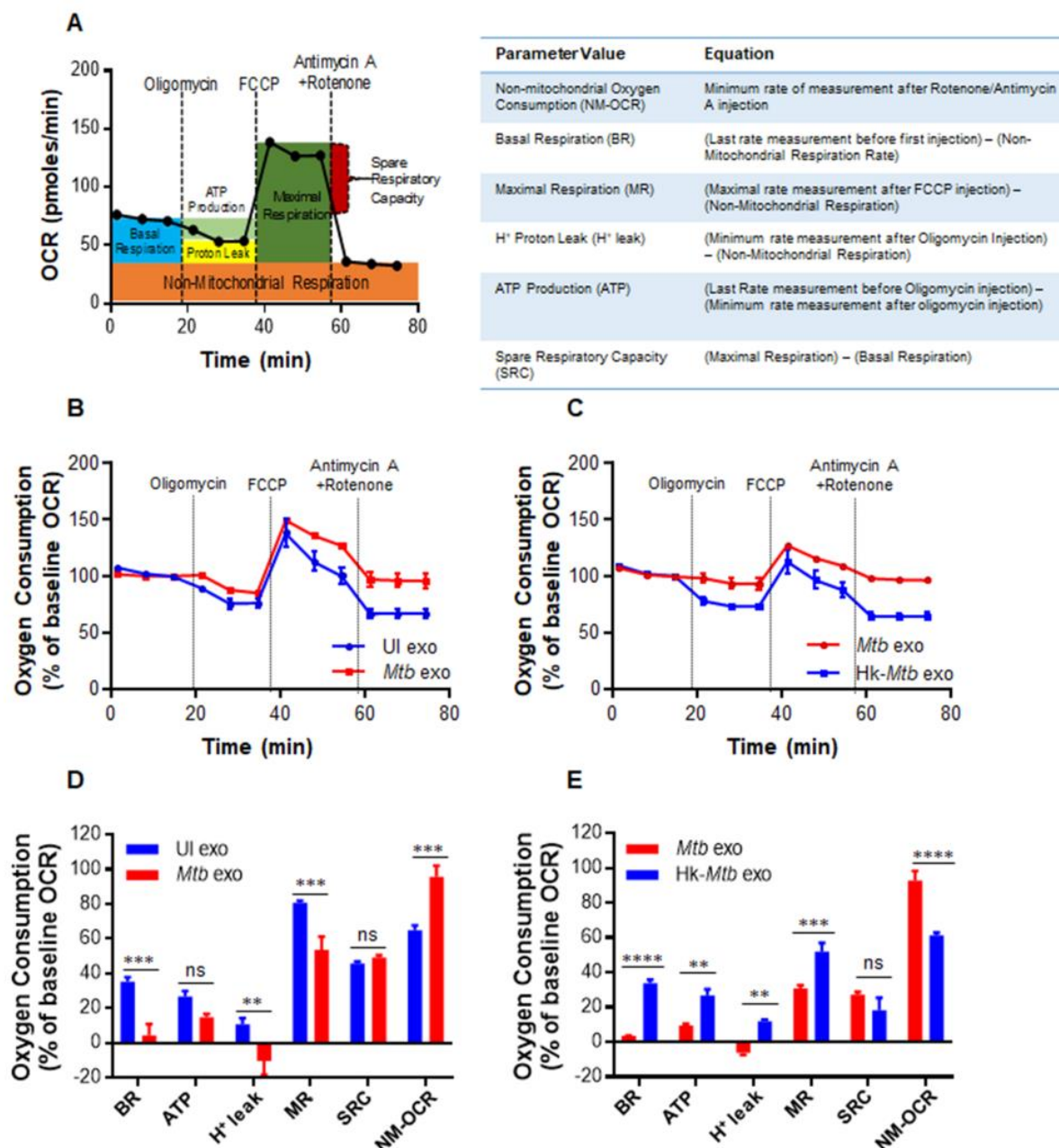
1425



1426
1427

1428 **Fig. 5. *Mtb* specific exosomes reactivate HIV-1 by inducing oxidative**
1429 **stress. (A)** RAW264.7 M ϕ were infected with *Mtb*, *Hk-Mtb*, Jal-1934 (MDR)
1430 and MYC431 (XDR) at moi 10. At 24 h p.i., exosomes were isolated from the
1431 culture supernatant, and 100 μ g/ml of exosomes were used to treat U1/Grx1-
1432 roGFP2 for 24 and 48 h. Ratiometric biosensor response was measured by
1433 flow cytometry. UI exo: denotes exosomes isolated from uninfected
1434 RAW264.7. **(B)** U1 cells were pre-treated with N-acetyl cysteine (NAC) for 1 h
1435 at indicated concentrations followed by exposure to *Mtb* specific exosomes
1436 (100 μ g/ml) for 24 h. HIV reactivation was measured by flow cytometry using
1437 fluorescent tagged antibody (PE labeled) specific to p24 (Gag) antigen. Data
1438 are representative of at least three independent experiments performed in
1439 triplicate. **(C)** U1 cells were treated with exosomes (100 μ g/ml) isolated from
1440 uninfected, *Mtb* infected, and *Hk-Mtb* infected RAW264.7. Total RNA from U1
1441 cells was isolated after 12 h of exosome treatment, followed by expression
1442 analysis of 185 genes specific to HIV host response and oxidative stress
1443 response utilizing NanoString customized gene expression panels. Data were
1444 normalized by nSolver (NanoString) software. Genes with significant changes
1445 were selected based on $p < 0.05$ and fold change > 1.5 between *Mtb* versus UI,
1446 *Mtb* versus *Hk-Mtb*, *Hk-Mtb* versus UI. Data is displayed as heat maps of
1447 three groups together. **(D)** Expression profile of HIV host response and
1448 oxidative stress response in U1 monocytes and U1 macrophages (PMA-
1449 differentiated). Error bars represent standard deviations from the mean.
1450 **** $p < 0.0001$ (two-way ANOVA). Data are representative of at least two
1451 independent experiments performed in duplicate.

1452



1453

1454 **Fig. 6. *Mtb*-specific exosomes modulate OXPHOS of U1 cells. (A)**

1455 Schematic presentation of Agilent Seahorse XF Cell Mito Stress test profile of

1456 the key parameters of mitochondrial respiration. **(B and C)** RAW264.7

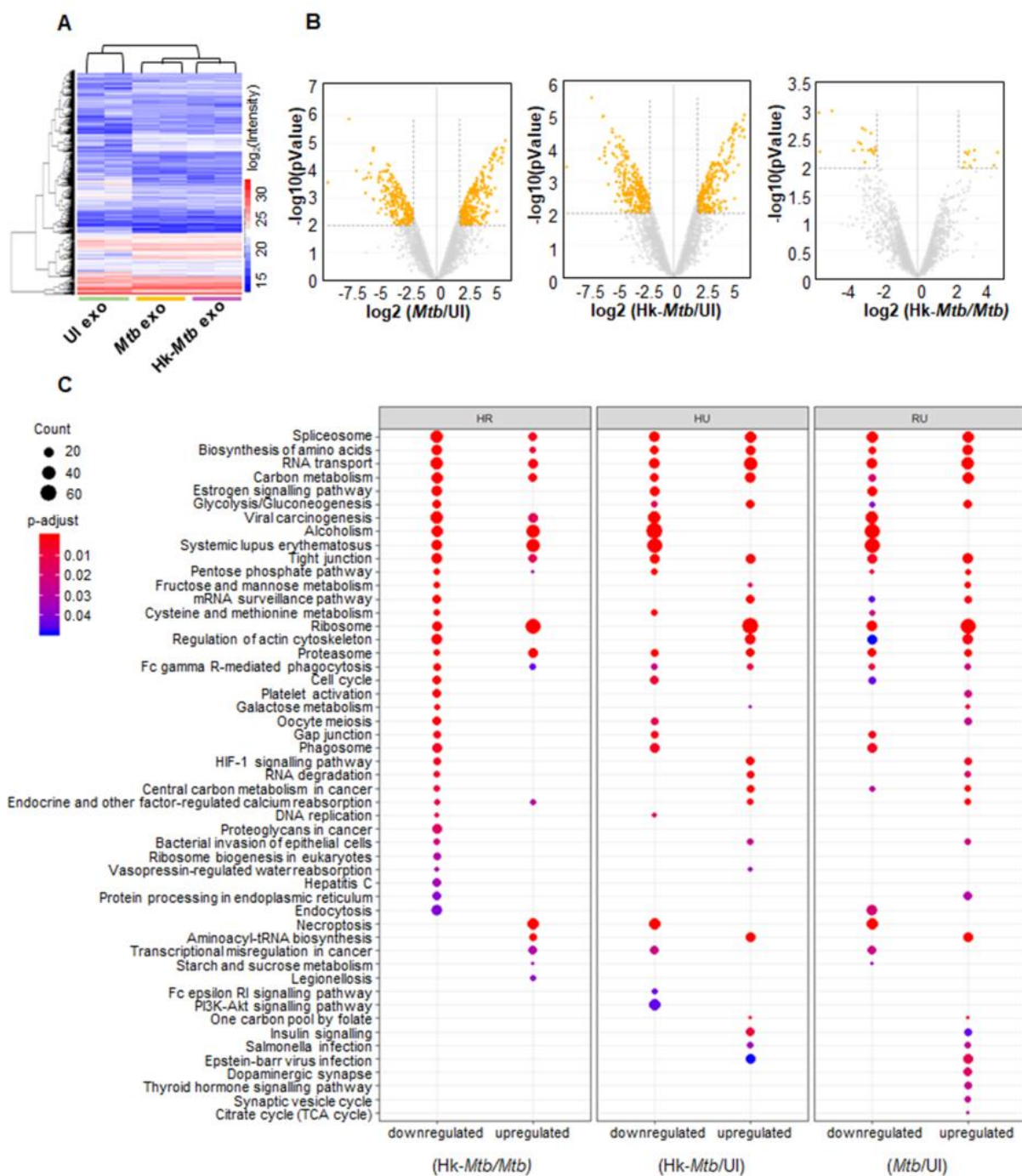
1457 macrophages were infected with *Mtb* and Hk-*Mtb* at moi 10. At 24 h p.i.,

1458 exosomes were isolated from the culture supernatant, and 100 µg/ml of

1459 exosomes were used to treat U1 for 48 h. Respiratory profile of U1 cells on

1460 treatment with exosomes isolated under indicated conditions. U1 exo:

1461 exosomes isolated from uninfected RAW264.7. Respiratory profile was
1462 measured and expressed as percent of basal oxygen consumption rate
1463 (%OCR). Oxygen consumption was measured without any inhibitor (basal
1464 respiration), followed by OCR change upon sequential addition of oligomycin
1465 (1 μ M; ATP synthase inhibitor) and cyanide-4
1466 [trifluoromethoxy]phenylhydrazone (FCCP; 0.25 μ M), which uncouples
1467 mitochondrial respiration and maximizes OCR. Finally, respiration was
1468 completely shut down by inhibiting respiration using antimycin A and
1469 Rotenone (0.5 μ M each), inhibit complex III and I, respectively. **(D and E)**
1470 Various respiratory parameters as outlined in the table of panel A were
1471 measured using the values obtained from the dataset depicted in panel **(B)**
1472 and **(C)** and as described in materials and methods. Error bars represent
1473 standard deviations from the mean. ns- non significant; **p<0.01; ***p<0.001
1474 (two tailed unpaired t-test). Data are representative of at least two
1475 independent experiments performed in triplicate.
1476



1477

1478 **Fig. 7. Proteomics of *Mtb* specific exosomes by LC-MS/MS. RAW264.7**

1479 *Mφ* were infected with *Mtb* and *Hk-Mtb* at moi 10 or left uninfected. At 24 h

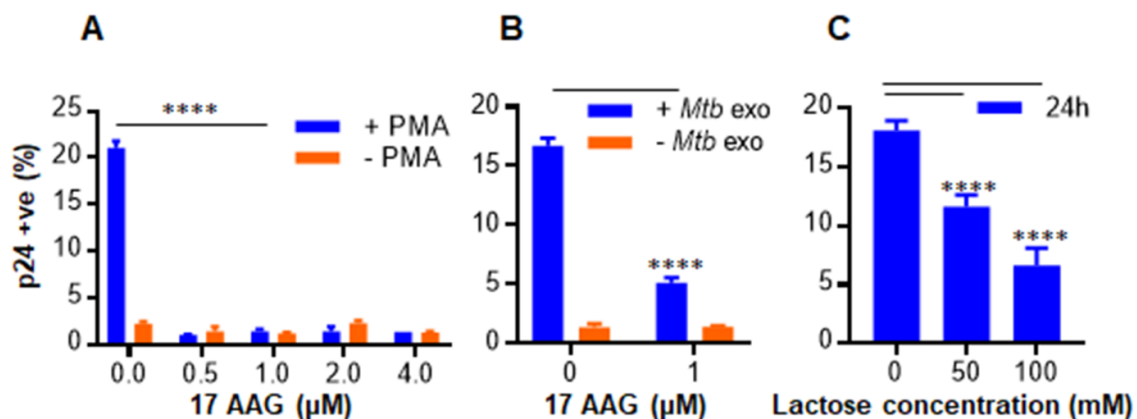
1480 p.i., exosomes were isolated from the culture supernatant for LC-MS/MS. **(A)**

1481 Heat map of differentially expressed proteins of exosomes in three samples.

1482 **(B)** Volcano plots of differentially expressed proteins. Significantly up-

1483 regulated and down-regulated proteins with log2 fold change more than two

1484 are shown as orange dots. **(C)** Enriched KEGG signaling pathways, proteins
1485 upregulated or downregulated in different comparison groups: (heat killed) Hk-
1486 *Mtb* versus live *Mtb*, Hk-*Mtb* versus UI (uninfected) and live *Mtb* versus UI
1487 (uninfected).



1488

1489 **Fig. 8. Hsp-90 and Galectin inhibitors reverse the exosomes mediated**

1490 **HIV-1 reactivation in U1 cells. (A)** U1 cells were stimulated with 5 ng/ml of

1491 PMA to induce HIV reactivation in presence of indicated concentration of 17-

1492 AAG (Hsp-90 inhibitor). **(B)** U1 cells were treated with 100 µg/ml of *Mtb*

1493 exosomes isolated from RAW264.7 as described earlier and HIV reactivation

1494 was monitored in the presence of indicated concentration of 17-AAG. **(C)** *Mtb*

1495 infected RAW264.7 macrophages were treated with 50 and 100 mM of

1496 lactose (galectins inhibitor) for 24 h and exosomes were isolated. These

1497 exosomes were then used to reactivate HIV-1 from U1 cells. HIV-1

1498 reactivation was measured by flow cytometry using fluorescent tagged

1499 antibody (PE labeled) specific to p24 (Gag) antigen. Error bars represent

1500 standard deviations from the mean. *p<0.05; **p<0.01; *** p<0.001;

1501 ****p<0.0001. One-way ANOVA **(C)** and two-way ANOVA **(A, B)**. Data are

1502 representative of at least two independent experiments performed in

1503 duplicate.

1504 **Supplementary Information**

1505

1506 **Mycobacterium tuberculosis reactivates HIV via exosomes mediated**

1507 **resetting of cellular redox potential and bioenergetics**

1508

1509 Priyanka Tyagi^{1, 2}, Virender Kumar Pal¹, Sandhya Srinivasan³, and Amit

1510 Singh^{1*}

1511 ¹Department of Microbiology and Cell Biology, Centre for Infectious Disease

1512 Research, Indian Institute of Science (IISc), Bangalore-12

1513 ²International Centre for Genetic Engineering and Biotechnology (ICGEB),

1514 New Delhi-67

1515 ³Vproteomics, New Delhi-16

1516

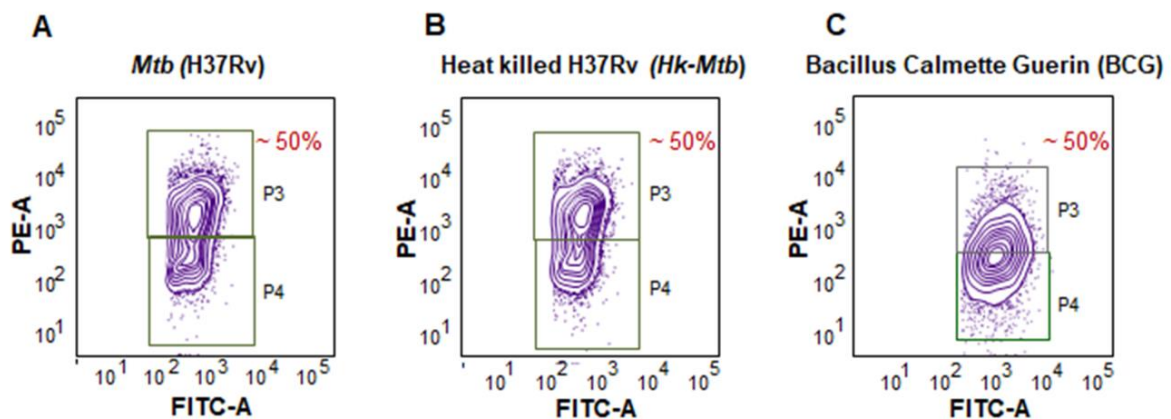
1517 Keywords: Exosomes, glutathione, redox potential, extracellular acidification

1518 rate, oxidative phosphorylation, roGFP

1519

1520

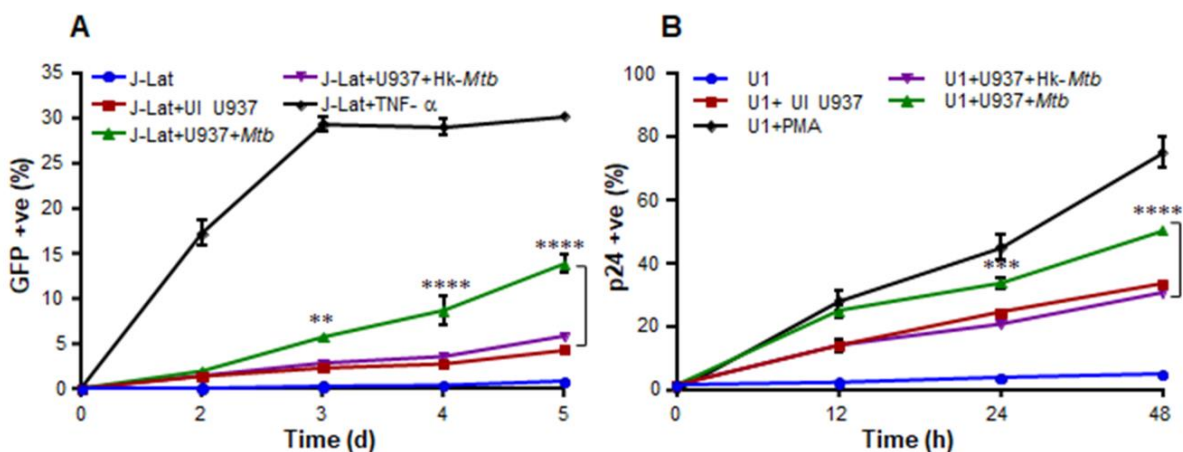
1521 **Supplementary figures:**
 1522



1523

1524 **Fig. S1. *Mtb* H37Rv, Heat killed H37Rv (*Hk-Mtb*), and BCG equally infect**
 1525 **the U937 Mφ.** PMA differentiated U937/Grx1-roGFP2 were infected with
 1526 PKH26 labeled bacilli (MOI 10). **(A-C)** Dot plot of U937/Grx1-roGFP2 after
 1527 infection with **(A)** H37Rv (*Mtb*), **(B)** (*Hk-Mtb*) and **(C)** Bacillus Calmette Guerin
 1528 (BCG). P3 represents *Mtb* infected U937 cell subpopulation and P4 represent
 1529 bystander U937 cell subpopulation.

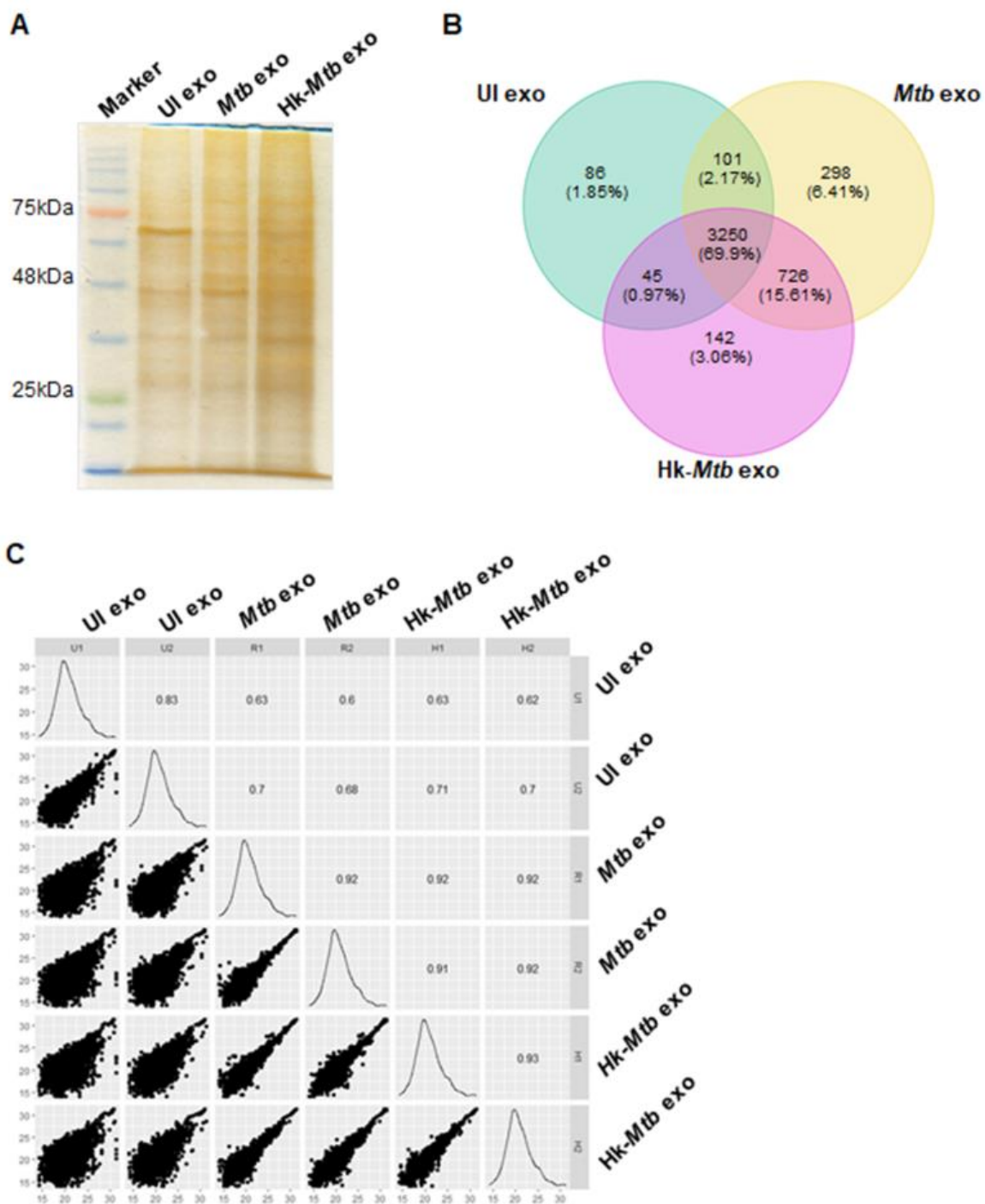
1530



1531

1532 **Fig. S2. *Mtb* infected Mφ reactivates latent HIV-1 from lymphocytes and**
 1533 **monocytes. (A)** J-Lat T cells are latently infected with the HIV-1 provirus
 1534 containing green fluorescent protein [GFP] in the genome. Reactivation of
 1535 HIV-1 can be easily monitored by measuring the increase in GFP

1536 fluorescence using flow cytometer. J-Lat cells were co-cultured with U937 Mφ
1537 pre-infected with live *Mtb* or *Hk-Mtb* for 4 h and GFP fluorescence was
1538 monitored at the indicated time points. GFP fluorescence of J-Lat cells treated
1539 with TNFα (10ng/ml) or left untreated was taken as the measure of
1540 reactivation or latency, respectively. As an additional control, J-Lat cells were
1541 also co-cultured with uninfected (UI) U937 Mφ. **(B)** U1 cells (U937 monocytes
1542 chronically infected with HIV-1), were co-cultured with UI, *Mtb* infected or Hk-
1543 *Mtb* infected U937 Mφ. At various time points, U1 cells were immuno-stained
1544 for intracellular HIV p24 (Gag) antigen and fluorescence response was
1545 measured by flow cytometry. Percent p24 antigen positive U1 cells
1546 corresponds to percent HIV reactivation upon co-culturing over time. PMA (5
1547 ng/ml) and U1 cells alone were used as positive and negative control,
1548 respectively. Error bars represent standard deviations from the mean. **
1549 p<0.01; ***p<0.001; **** p<0.0001 (two-way ANOVA). Data are representative
1550 of at least three independent experiments performed in triplicate.
1551



1552

1553 **Fig. S3. Proteomics of *Mtb* specific exosomes by LC-MS/MS. RAW264.7**

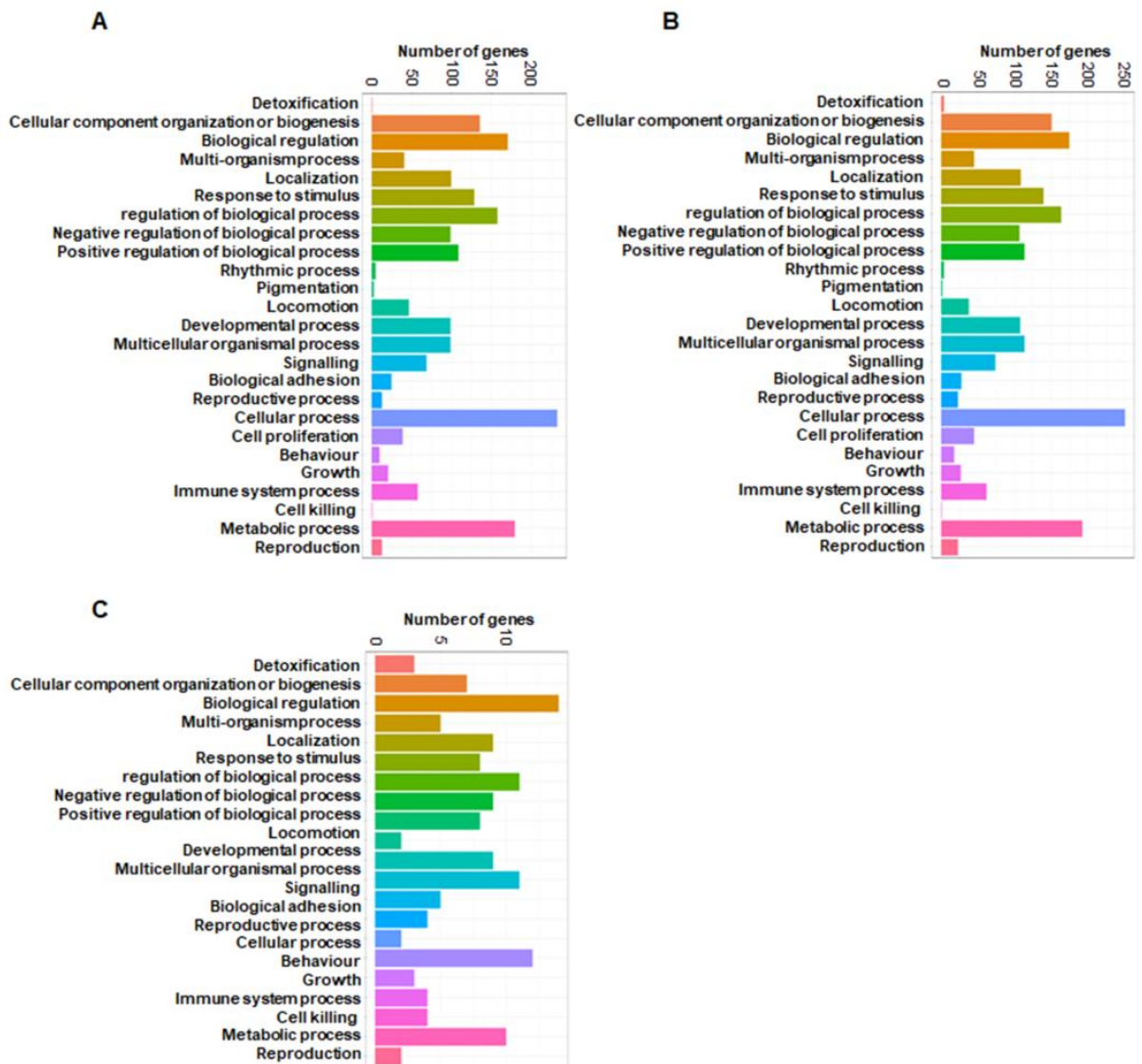
1554 Mφ were infected with *Mtb* and Hk-*Mtb* at moi 10 or left uninfected. At 24 h

1555 p.i., exosomes were isolated from the culture supernatant for LC-MS/MS. **(A)**

1556 Silver stained SDS-PAGE gel loaded with 10 μg of total exosomal protein. **(B)**

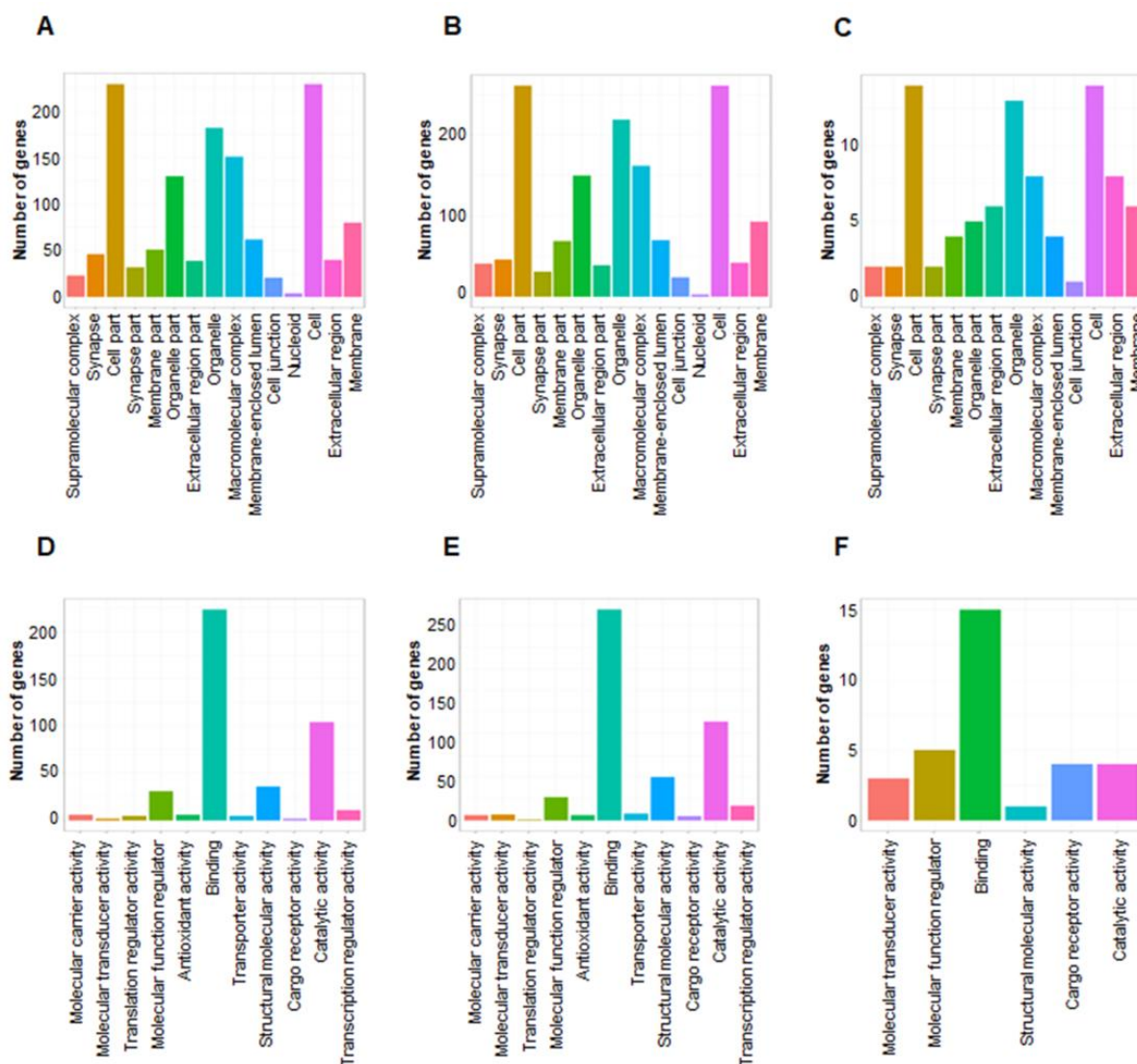
1557 Venn diagram showing percent overlap between the exosomal proteins

1558 identified by LC-MS/MS among three samples. **(C)** Correlation plot of three
 1559 exosome samples in duplicate.



1560

1561 **Fig. S4. Functional classification of differentially expressed proteins of**
 1562 **exosomes. (A)** Enriched GO terms (biological processes) of differentially
 1563 expressed proteins in *Mtb* exosomes *versus* UI exosomes. **(B)** Enriched GO
 1564 terms (biological processes) of differentially expressed proteins in Hk-*Mtb*
 1565 exosomes *versus* UI exosomes. **(C)** Enriched GO terms (biological
 1566 processes) of differentially expressed proteins in *Mtb* exosomes *versus* Hk-
 1567 *Mtb* exosomes.



1568

1569 **Fig. S5. Functional classification of differentially expressed proteins of**
 1570 **exosomes. (A)** Enriched GO terms (Cellular localization) of differentially
 1571 expressed proteins in *Mtb* exosomes *versus* UI exosomes. **(B)** Enriched GO
 1572 terms (Cellular localization) of differentially expressed proteins in Hk-*Mtb*
 1573 exosomes *versus* UI exosomes. **(C)** Enriched GO terms (Cellular localization)
 1574 of differentially expressed proteins in *Mtb* exosomes *versus* Hk-*Mtb*
 1575 exosomes. **(D)** Enriched GO terms (Molecular Function) of differentially
 1576 expressed proteins in *Mtb* exosomes *versus* UI exosomes. **(E)** Enriched GO
 1577 terms (Molecular Function) of differentially expressed proteins in Hk-*Mtb*
 1578 exosomes *versus* UI exosomes. **(F)** Enriched GO terms (Molecular function)

1579 of differentially expressed proteins in *Mtb* exosomes versus *Hk-Mtb*
1580 exosomes.

1581

1582 **Tables**

1583 **Table S1**

1584 **Table S1a.** List of genes used for nCounter Gene Expression Assay.

1585 **Table S1b.** Normalized intensity values of differentially expressed gene in
1586 nCounter Gene Expression Assay.

1587 **Table S1c.** Normalized intensity values of differentially expressed gene in
1588 nCounter Gene Expression Assay.

1589

1590 **Table S2.** List of proteins identified in LC/MS-MS of uninfected, live H37Rv
1591 (*Mtb*) and heat killed H37Rv (*Hk-Mtb*) exosomes.

1592

1593 **Table S3**

1594 **Table S3a.** List of differentially expressed proteins in live H37Rv (*Mtb*) versus
1595 Uninfected (UI) exosomes shown in volcano plots.

1596 **Table S3b.** List of differentially expressed proteins in heat killed H37Rv (*Hk-*
1597 *Mtb*) versus Uninfected (UI) exosomes shown in volcano plots.

1598 **Table S3c.** List of differentially expressed proteins in heat killed H37Rv (*Hk-*
1599 *Mtb*) versus live H37Rv (*Mtb*) exosomes shown in volcano plots.

1600

1601 **Table S4**

1602 **Table S4a.** Biological process Gene ontology (GO) term enrichment analysis
1603 of live *H37Rv (Mtb)* versus Uninfected (UI) exosome proteins.

1604 **Table S4b.** Cell localisation Gene ontology (GO) term enrichment analysis of
1605 live *H37Rv* (*Mtb*) versus Uninfected (UI) exosome proteins.

1606 **Table S4c.** Molecular function Gene ontology (GO) term enrichment analysis
1607 of live *H37Rv* (*Mtb*) versus Uninfected (UI) exosome proteins.

1608

1609 **Table S5**

1610 **Table S5a.** Biological process Gene ontology (GO) term enrichment analysis
1611 of heat killed *H37Rv* (*Hk-Mtb*) versus Uninfected (UI) exosome proteins.

1612 **Table S5b.** Cell localisation Gene ontology (GO) term enrichment analysis of
1613 heat killed *H37Rv* (*Hk-Mtb*) versus Uninfected (UI) exosome proteins.

1614 **Table S5c.** Molecular function Gene ontology (GO) term enrichment analysis
1615 of heat killed *H37Rv* (*Hk-Mtb*) versus Uninfected (UI) exosome proteins.

1616

1617 **Table 6**

1618 **Table S6a.** Biological process Gene ontology (GO) term enrichment analysis
1619 of live *H37Rv* (*Mtb*) versus Heat killed *H37Rv* (*Hk-Mtb*) exosome proteins.

1620 **Table S6b.** Cell localisation Gene ontology (GO) term enrichment analysis of
1621 live *H37Rv* (*Mtb*) versus Heat killed *H37Rv* (*Hk-Mtb*) exosome proteins.

1622 **Table S6c.** Molecular function Gene ontology (GO) term enrichment analysis
1623 of live *H37Rv* (*Mtb*) versus Heat killed *H37Rv* (*Hk-Mtb*) exosome proteins.

1624

1625 **Table S7.** KEGG pathway enrichment analysis of heat killed *H37Rv* (H)
1626 exosomes versus live *H37Rv* (R) exosomes, heat killed *H37Rv* (H) exosomes
1627 versus Uninfected (U) exosomes, live *H37Rv* (R) versus Uninfected (U)
1628 exosome proteins.